nature communications



Article

https://doi.org/10.1038/s41467-025-61312-0

Pericyte pannexin1 controls cerebral capillary diameter and supports memory function

Received: 11 January 2024

Accepted: 16 June 2025

Published online: 03 July 2025



Check for updates

Sandra Mai-Morente 1, Eugenia Isasi, Alberto Rafael, Gonzalo Budelli, Silvia Olivera-Brayo⁴, Nathalia Vitureira¹ & Verónica Abudara D¹

In the blood-brain-barrier, contractile pericytes fine-tune the capillary resistance and blood supply to meet neuro-metabolic demands; molecular players governing these functions remain unclear. Here we show that mice cerebral pericytes express functional pannexin1 (Panx1) channels, which drive efflux of ATP, a key activator of pericyte contractility. In hippocampal slices, pericyte Panx1 mediates capillary diameter changes in response to extracellular ATP fluctuations and glutamatergic synaptic transmission, known to contribute functional hyperaemia. Pharmacological inhibition of Panx1 in mice induces capillary widening in the cortex and hippocampus. Genetic deletion of pericyte Panx1 disrupts learning-evoked capillary dilation and memory performance. Mechanistically, glutamatergic NMDA/AMPA and purinergic P2X7/ P2Y6 receptors modulate pericyte Panx1 activity, which ultimately adjusts ATP release, pericyte Ca²⁺ signalling and capillary dynamics. Our study unveils pericyte Panx1 as a physiological regulator of cerebral capillary diameter, which sustains brain function and serves as a potential therapeutic target for cerebrovascular cognitive disorders.

Information processing in the brain is energetically challenging. To meet metabolic demands, the cerebral blood flow (CBF) increases in active brain areas¹. This response, known as functional hyperaemia, outcomes from decreased cerebrovascular resistance following relaxation of arteriolar smooth muscle cells and capillary pericytes2-8.

Capillaries control the cerebrovascular resistance and serve as primary sites for gas and nutrient exchange between the bloodstream and the brain⁹. Among the constituents of the neurovascular unit, pericytes act as exclusive regulators of the capillary diameter. These cells express contractile proteins that allow them to modulate their tone in response to neuronal energy demands, thereby adjusting the CBF¹⁰. Changes in calcium (Ca²⁺) signaling drive pericyte contractility¹¹⁻¹⁵; yet, transitions in the polymerization and depolymerization states of actin may also regulate the pericyte tone¹⁶.

Despite current progress concerning the mechanisms coupling the brain microenvironment to vascular physiology, we still lack a comprehensive understanding of molecular factors governing the capillary resistance and how the latter interacts with the cerebral milieu. In recent years, compelling evidence has underscored the fundamental role of large-pore membrane channels formed of the protein subunit pannexin1 (Panx1), as crucial conduits for autocrine and paracrine signaling¹⁷⁻¹⁹. The Panx1 channels facilitate communication among neurons, glial cells, and blood vessels, regulating vascular structure and physiology²⁰⁻²². The Panx1 assembles into heptameric channels, which feature a significant central pore that operates as a physiological pathway for non-vesicular release of ATP, a key

¹Departamento de Fisiología, Facultad de Medicina, Universidad de la República, Montevideo, Uruguay. ²Departamento de Histología y Embriología, Facultad de Medicina, Universidad de la República, Montevideo, Uruguay. ³Departamento de Biofísica, Facultad de Medicina, Universidad de la República, Montevideo, Uruguay. ⁴Departamento de Neurobiología y Neuropatología, Instituto de Investigaciones Biológicas Clemente Estable (IIBCE), Montevideo, Uruguay. e-mail: abudara@fmed.edu.uy

modulator of vessel resistance^{3,23-25}. Consistently, Panx1 is found in smooth muscle cells of major systemic vessels, where it modulates the peripheral resistance and blood flow²⁶.

In pericytes, ATP triggers constriction, increasing resistance to capillary blood flow by raising intracellular Ca²⁺ levels through the activation of purinergic cationic ligand-gated (P2X1/7) and metabotropic G protein-coupled receptors (P2Y2/4/6)^{3,23,27,28}. Recent studies show that microglial interactions with capillaries via Panx1 and P2Y12 channels regulate CBF²². Here, we hypothesize that, if Panx1 is expressed by pericytes, it might fine-tune the pericyte tone by controlling the local release of ATP, ultimately adjusting the capillary diameter and blood flow. Besides, a potential role of pericyte Panx1 in capillary physiology could impact the brain function. Although recent transcriptomic investigations have indicated the presence of Panx1 mRNA in rodent pericytes²⁹, the expression of this protein in brain pericytes and its influence on cerebral functioning have yet to be investigated.

In this work, by using transgenic mice with global and pericyte deletion of Panx1, combined with pharmacological, immunological, and functional approaches, we assess the role of pericytes as cellular regulators of cerebral capillary dynamics and memory, focusing on Panx1 as a molecule underlying these functions.

Results

Brain capillary pericytes express functional Panx1 channels, which allow a molecular exchange with the cerebral microenvironment

Our study focused on hippocampal pericytes situated at and beyond the 4th branch, in proximity to arterioles or within the mid-capillary region, as illustrated (Fig. 1a, b) and reported³⁰. These include both ensheathing and thin-strand pericytes^{31,32}. To evidence a molecular transfer between pericytes and the surrounding cerebral milieu mediated by Panx1 channels, we investigated the uptake of the Panx1permeant dye, ethidium bromide (Etd⁺), in acute hippocampal slices from wild-type (WT) mice. In resting conditions, pericytes with active large-pore membrane channels incorporated the dve and displayed Etd⁺ fluorescence (Fig. 1c-f). Pericytes at vessel axes and bifurcations demonstrated comparable levels of dye-uptake (Fig. 1g-i). To compensate for the lack of vascular tone in slices, we applied norepinephrine at a pre-contracting concentration (NE, 1.5 µM) in presence of ascorbate (100 µM), which delays NE oxidation³³. No significant differences in pericyte Etd+-uptake were observed between precontracted and non-precontracted slices (Fig. 1i). Ensheathing and thin-strand capillary pericytes captured similar levels of dye (Fig. 1j). To identify the molecular identity of the large-pore channels mediating dye influx, we examined the pharmacological sensitivity of Etd⁺-uptake to connexin hemichannel (CxHC) and pannexin (Panx) channels inhibitors in WT and global KO Panx1^{-/-} mice. The general Cx/Panx channel blocker carbenoxolone (CBX; 100 μM)³⁴ induced a comparable reduction in dye-uptake among WT hippocampal pericytes from both non-precontracted (47%) and precontracted (53%) slices (Fig. 1k-s). Aligned with this, pericytes from global KO Panx1^{-/-} mice exhibited 50% less Etd⁺ fluorescence compared to WT mice (Fig. 2a). This finding suggested that pericytes express open Panx1 channels under resting conditions. Accordingly, lanthanum (La³⁺; 200 µM), a general CxHC blocker with little effect on Panx1, did not alter dye-uptake by pericytes in hippocampal slices, whereas probenecid (PBD; 500 µM), a Panx1 inhibitor that does not affect Cxs^{34,35} significantly blocked uptake (62%) by WT pericytes. Mimetic peptides interact with the extracellular loops of Cxs/Panxs, inhibiting them; Gap26 (150 µM), which specifically inhibits Cx43-formed HCs and gap junctions³⁶, and Gap19 (150 μM), a selective Cx43HC blocker³⁷ produced no changes. Like PBD, the mimetic peptide Panx1 blocker, ¹⁰Pannexin1 (¹⁰Panx1; 150 µM)¹⁸, significantly attenuated uptake (59%), while the scrambled peptide, ScrPanx1, was ineffective (Fig. 2b, c). Thus, Panx1 channels are main contributors to basal Etd⁺ permeability in hippocampal pericytes.

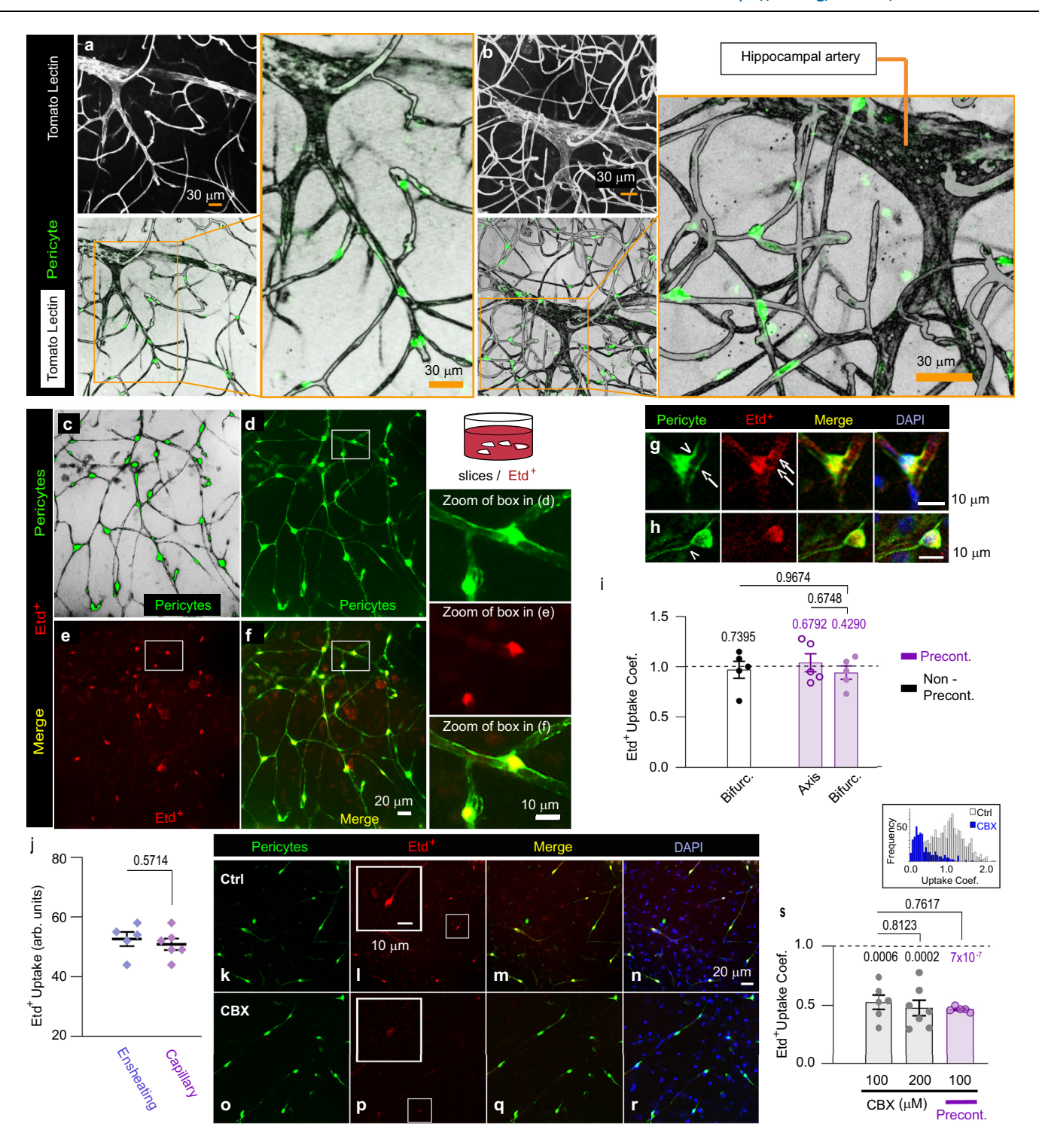
Consistent with this, genetic suppression of Panx1 in global knockout Panx1 (KO Panx1 $^{-/-}$) mice precluded blocking effects of CBX (100 μ M) and mimetic peptide 10 Panx1 (150 μ M) when compared to non-treated slices, whereas the Cx43HC blocker Gap19 (150 μ M) was ineffective (Fig. 2c).

To establish that the Panx1 channels responsible for the transmembrane exchange are those particularly expressed by pericytes, we followed different strategies. Initially, we evaluated pericyte dyeuptake in hippocampal slices from conditional mice whose Panx1 was suppressed in pericytes. To achieve this, we generated tamoxifeninducible pericyte Panx1-deleted (Pdgfrb.Panx1 $^{\Delta/\Delta}$) mice (Fig. 2d); the efficiency and specificity of Panx1 deletion in pericytes was determined by immune and functional studies (see "Assessment of Panx1 deletion" in Methods section). Pericytes from conditional Pdgfrb.Panx1^{Δ/Δ} mice exhibited less Etd+ fluorescence (46%) compared to pericytes from age-matched littermates not expressing the Cre recombinase transgene (Pdgfrb.CRE-/Panx1fl/fl mice) (Fig. 2e). As in WT slices, Panx1 blockers CBX (100 μM) and mimetic peptide ¹⁰Panx1 (150 μM) reduced uptake (by respectively 51% and 52%) by hippocampal pericytes derived from Pdgfrb.CRE-/Panx1^{fl/fl} mice, whereas the Cx43HC blocker Gap19 was ineffective. Like in global KO Panx1^{-/-} mice, the Cx/Panx blockers failed to affect Etd+uptake by hippocampal pericytes in conditional Pdgfrb.Panx1^{Δ/Δ} mice, suggesting that Panx1 channels expressed by pericytes mediated dye-transfer (Fig. 2f). As indirect evidence of the functionality of pericyte Panx1 channels in freely moving mice, we administered an intraperitoneal injection of PBD (200 mg/kg; i.p.), a known in vivo blocker of brain Panx138, and conducted dye-uptake in ex vivo acute slices (Fig. 2g, h). Probenecid reduced Etd⁺-uptake (46%) compared to mice receiving the vehicle (Fig. 2h). The PBD-sensitive components of uptake under both in vivo and ex vivo conditions were similar (Fig. 2i), further attesting that healthy awake mouse expresses basally open pericyte Panx1 channels.

Then, we assessed Etd+-uptake in rat primary cultures, which contain a minimum of 95% cerebral pericytes; these express neural/ glial antigens 2 (NG2) and platelet-derived growth factor receptor beta (PDGFRβ)³⁹. Unlike thin-strand pericytes in situ, most of these cultured cerebral pericytes also express alpha-smooth muscle actin (aSMA; Supplementary Fig. 1). Consistent with pericytes presenting functional Panx1 channels, cultures exhibited decreased uptake when treated with Panx1 blockers, CBX (44%) and 10Panx1 (45%) and unaltered uptake when exposed to the Cx43HCs blocker Gap19 (Supplementary Fig. 2). Next, we addressed the cellular distribution of Panx1 in pericytes, endothelium, vascular smooth muscle cells (SMCs) and neurons of hippocampal slices from different mouse strains, WT, Pdgfrb.CRE-/ Panx1^{fl/fl}, conditional Pdgfrb/Panx1^{Δ/Δ}, and global KO Panx1^{-/-}. Panx1 immunofluorescence stained the majority of endothelial cells, vascular SMCs, and CA1 neurons in all strains except for global Panx1^{-/-} knockout mice, as well as the membrane and cytosol of pericytes in WT and Pdgfrb.CRE-/Panx1fl/fl mice (Supplementary Figs. 3 and 4). No Panx1 signal was detected in the majority of pericytes from conditional Pdgfrb/Panx1^{\(\Delta\)} and global Panx1^{-/-} knockout mice, both of which displayed similar levels of Panx1 suppression (Supplementary Fig. 3a-c). Cultured murine cerebral pericytes exhibited a similar Panx1 immunofluorescence distribution as pericytes from hippocampal slices (Supplementary Fig. 3d). Besides, Western blotting revealed bands migrating at ~35-50 kDa, likely representing post-translational glycosylation of Panx1 (Supplementary Fig. 3e)40,41. Collectively, pharmacological, genetic, and immunological approaches showed that pericytes express active Panx1 channels under physiological conditions, facilitating molecular exchange with the brain environment.

Cerebral pericyte Panx1 channels are molecular routes for ATP release that amplify pericyte Ca²⁺ signaling

ATP promotes capillary constriction by enhancing pericyte Ca²⁺ and contractility^{3,23,28,42,43}. If pericyte Panx1 channels allow ATP release,



changes in Panx1 channels activity are predicted to impact local extracellular ATP levels, intracellular Ca²⁺, and pericyte tone. We then determined whether pericyte Panx1 channels behave as ATP-releasing routes in primary cultures of rat cerebral pericytes. The amount of ATP measured in media derived from pericyte cultures treated with mimetic peptide ¹⁰Panx1 (150 μM) was decreased by 4.3-fold when compared to untreated cultures (Fig. 3a), suggesting that endogenous ATP originated from pericytes is basally discharged through open Panx1 channels. Next, we investigated whether Panx1 activity could modulate pericyte Ca²⁺. Selective blocking of pericyte Panx1 with ¹⁰Panx1 (150 μM) reduced the baseline intracellular Ca²⁺ fluorescence [both maximum change and area under the curve per minute (AUC/

min)] (Fig. 3b, c), suggesting that Panx1 channels functionality contributes to set basal pericyte Ca²⁺ levels, likely through release of endogenous ATP. Application of exogenous ATP (100 μ M) enhanced the fluorescence Ca²⁺ signal [both maximum change and area under the curve per minute (AUC/min)] and triggered Ca²⁺ oscillations in pericytes (Fig. 3d–h). The Panx1 inhibitor 10 Panx1 (150 μ M) reduced the ATP-evoked Ca²⁺ responses to near baseline levels (Fig. 3i–l). Collectively, these findings suggest that cerebral pericyte Panx1 channels mediate ATP release and amplify pericyte Ca²⁺ levels. In other systems, purinoreceptors activate Panx1 channels to release ATP, which in turn stimulates additional purinoreceptors $^{4+}$. This functional link might be required for recruiting more active ATP-releasing Panx1 channels and

Fig. 1 | Hippocampal capillary pericytes communicate with the extracellular cerebral milieu via large-pore membrane channels. a, b Fluorescent views of the hippocampal artery and its ramifications. Below, the corresponding inverted images are superimposed with fluorescently TO-PRO™-3-labeled pericytes. The regions within the orange boxes were zoomed and are shown on the right. c-f Fluorescent capillary pericytes from hippocampal slices capture the hemichannel-permeant tracer Etd+ in resting conditions (Stratum Radiatum, same field); in pseudo-colored image (c), prolongations originated from pericyte somas intermingle. Superimposed images (d, e) show Etd+-labeled pericytes (yellow, f); boxes areas in (d-f) were zoomed and are shown on the right. Fluorescent micrographs show two TO-PROTM-3-positive Etd⁺-labeled pericytes localized in adjacency to a vascular bifurcation (g) or axis (h). Longitudinal primary prolongations (arrow heads) originated from pericyte somas run along the capillary axis; secondary circular prolongations (arrows) derived from primary prolongations surround the vessel. i Etd*-uptake coefficients of pericytes contiguous to vascular axes and bifurcations in nonprecontracted (bifurcations, n = 5) and precontracted (NE 1.5 uM plus ascorbate 100 μM) (axis, n = 5; bifurcations, n = 5) hippocampal slices. All data were

normalized relative to non-precontracted axis (dashed line; n = 5). Two-tailed onesample t-test, each condition compared to non-precontracted axis (p values over bars); one-way-ANOVA with post-hoc Tukey (between indicated conditions). j Etd*uptake (arbitrary units) by ensheating (n = 5) and thin-strand (n = 6) pericytes show no differences; unpaired two-tailed t-test (between indicated groups). Fluorescent microphotographs display inhibited Etd*-uptake by hippocampal pericytes treated with carbenoxolone (CBX); (Ctrl; same field, k-n) and (CBX 100 μM; same field, o−r). Boxes in (I, p) were zoomed. s The CBX decreases Etd+-uptake coefficients of pericytes from non-contracted (CBX 100 μ M, n = 6; CBX 200 μ M, n = 7) and precontracted (CBX 100 μ M, n = 5) hippocampal slices compared to control (dashed line; n = 7). All data were normalized relative to non-precontracted control. Twotailed one-sample t-test, compared to control (p over bars); one-way-ANOVA with post-hoc Tukey, between indicated conditions. Inset: Frequency distribution (bin 0.05) of Etd $^+$ -uptake coefficients for control (n = 13) and CBX (100 μ M)-treated (n=8) pericytes. In (i, j, s), data are presented as mean \pm SEM. (n) number of mice. Source data are provided as a Source Data file.

purinoreceptors, thereby amplifying pericyte Ca²⁺ signaling through a feed-forward loop as proposed elsewhere⁴⁵. We then explored a potential functional relationship between Panx1 channels and purinoreceptors in brain pericytes.

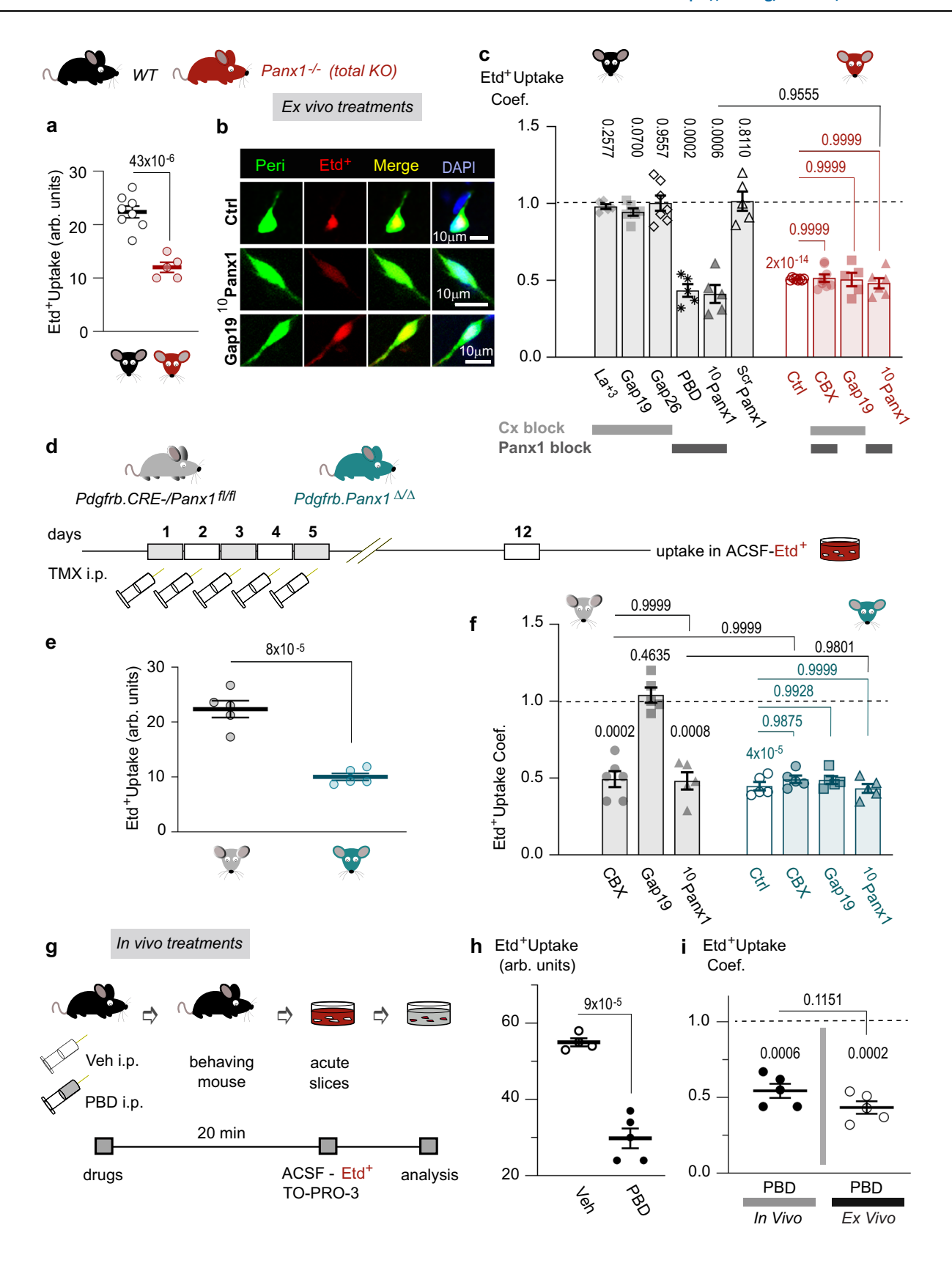
Extracellular ATP fluctuations regulate pericyte Panx1 channel activity through ionotropic P2X7 and metabotropic P2Y6 purinoreceptors

According to our findings, cerebral pericytes express functional Panx1 channels, which sustain ATP release. In other systems, ATPstimulated ligand-gated ionotropic and metabotropic purinoreceptors activate Panx1 channels⁴⁴. Hence, we investigated whether purinergic signaling regulates pericyte Panx1. Initially, we explored the contribution of endogenous ATP by applying the soluble ATPase apyrase (Apy, 8 U/ml) to WT hippocampal slices. Apy decreased dyeuptake (60%) in WT pericytes but was ineffective in KO Panx1^{-/-} mice suggesting that endogenous ATP contributes pericyte Panx1 channels basal activity (Fig. 4a). Deletion of Panx1 in pericytes confirmed this finding in conditional Pdgfrb/Panx1^{Δ/Δ} mice, demonstrating the involvement of Panx1 expressed in pericytes (Supplementary Fig. 5). Simultaneous application of non-selective P2Xr and P2Yr antagopyridoxalphosphate-6-azophenyl-2',4'-disrespectively nists. ulphonic acid (PPADS, 50 μM) and Reactive Blue-2 (RB2, 100 μM)^{46,47} reduced uptake by 77% which exceeded the inhibition induced by PPADS alone (42%). These effects were blunted in KO Panx1^{-/-} mice. Thus, both ionotropic P2Xr and metabotropic P2Yr contribute to basal Panx1 channel-dependent permeability (Fig. 4a). Since ATPgated cation P2X7R activates Panx1 in macrophages¹⁸ and constricts pericytes²³, we tested the pharmacological sensitivity of pericyte uptake to selective P2X7R blockers, the non-competitive Brilliant Blue G (BBG)⁴⁸ and competitive [3H]2-cyano-1-[(1S)-1-phenylethyl]-3quinolin-5-ylguanidine (A804598)⁴⁹; these inhibitors reduced uptake by, respectively, 44% and 47% at 5 μM (Fig. 4b). Since pericytes express metabotropic P2Y6R²⁷ which triggers ATP release via Panx1 channels in urothelium⁵⁰, we tested the selective P2Y6R antagonist, 1-(3-isothiocyanatophenyl)-3-[4-[(3-isothiocyanatophenyl)carbamothioylamino]butyl] thiourea (MRS2578)⁵¹ in hippocampal pericytes; MRS2578 evoked a dose-dependent inhibition of dye-uptake with E_{50} ~5 μ M (37% reduction). Consistent with P2X7R and P2Y6R supporting basal pericyte Panx1 activity, inhibitory effects of purinergic blockers on dye-uptake were rescued to near control in Panx1^{-/-} mice (Fig. 4b, c). The simultaneous application of the same dose (5 µM) of A804598 and MRS2578 resulted in a 79% inhibition (Supplementary Fig. S6a), which is comparable to the combined effect (84%) of each blocker applied separately. As expected, immunofluorescence of P2X7R and P2Y6R was detected at the pericyte membrane in the hippocampus (Supplementary Fig. 6b-d).

Next, we assessed how exogenous ATP affects pericyte Panx1 channels. Application of ATP (0.05-5 mM) to acute WT hippocampal slices generated a dose-dependent increase in pericyte dye-uptake. Maximum uptake increase (49%) occurred at 100 μM ATP; noteworthy, with higher concentrations (i.e., 5 mM), uptake increase declined. Suppression of Panx1 rescued uptake values near to control for 0.1 and 5 mM ATP in Panx1^{-/-} mice evidencing that Panx1-mediated ATPinduced uptake (Fig. 4e); deletion of Panx1 in pericytes confirmed this finding in conditional Pdgfrb/Panx1^{Δ/Δ} mice, demonstrating the involvement of Panx1 expressed in pericytes (Supplementary Fig. 5). In presence of ATP (100 µM), purinergic blockers, A804598 (5 µM) and MRS2578 (5 µM) reduced dye-uptake in WT pericytes by 80% and 87%, respectively, and by 103% when applied together. This effect was suppressed in Panx1^{-/-} mice (Fig. 4f). These uptake-sensitive components to purinergic blockers in presence of ATP were larger than in its absence (A804598, 47%; MRS2578, 37%; A804598 + MRS2578, 79%), suggesting that ATP-induced uptake increase involved activation of Panx1 through P2X7R/P2Y6R signaling. In accordance, treating slices with 2'(3')-O-(4-benzoylbenzoyl)adenosine 5'-triphosphate (BzATP; 1μM) a non-hydrolysable selective P2X agonist which potently stimulates P2X7R⁵² and with the selective P2Y6R agonist uridine 5'-diphosphate (UDP; 100 μM)⁵³, increased dye-uptake (by 20% and 34%, respectively). Suppression of Panx1 rescued uptake to near control in Panx1^{-/-} mice demonstrating the involvement of Panx1 channels (Fig. 4g). Treating cerebral pericyte cultures with Apy, ATP and purinergic blockers A804598 and MRS2578, produced comparable results to those obtained in hippocampal slices suggesting a direct effect of ATP on pericyte purinoreceptors (Supplementary Fig. 7). Altogether, our data indicate that ATP, either endogenously released or exogenously applied, open pericyte Panx1 channels through pericyte ionotropic P2X7R and metabotropic P2Y6R. However, the involvement of additional purinoreceptor subtypes cannot be discarded.

Extracellular ATP fluctuations regulate hippocampal capillary diameters, with capillary responses requiring Panx1 expression by pericytes

Our results suggest that extracellular ATP opens pericyte Panx1 channels, which facilitate ATP release, reinforcing extracellular ATP levels near the pericyte's membrane. Since ATP constricts capillaries, we predict that Panx1 could modulate capillary responses to changes in endogenous or exogenous ATP. To demonstrate this, we determined diameters as a function of the distance from the pericyte soma in fluorescently tagged capillaries from hippocampal slices (Fig. 5a–e). Following a 15-min treatment with apyrase (Apy; 8 U/ml), capillary diameter near pericyte somata in WT slices increased by 18% compared to control (untreated) vessels, while mean capillary diameter at remote regions (>5 µm from the pericyte center) remained unchanged



between control and Apy-treated slices (two-tailed unpaired t-test) (Fig. 5c, e). This agrees with previous reports that emphasize the major influence of pericyte somata on capillary diameter^{54,55}. In Pdgfrb.Panx1^{A/A} mice, suppression of Panx1 in pericytes, abolished the Apy-evoked dilation at pericyte soma observed in WT slices (Fig. 5d, e), suggesting that Panx1 expressed in pericytes mediated Apy-dilation. As

a complementary approach, we assessed the diameter change between pericyte and non-pericyte sites within same capillaries in control and Apy-treated slices (Fig. 5f-j). Accordingly, Apy increased the capillary diameter between pericyte and non-pericyte sites in WT mice compared to control (18.2%), an effect that was suppressed in Pdgfrb.Panx1^{Δ/Δ} mice (Fig. 5h-j), corroborating the role of pericyte

Fig. 2 \mid Panx1 channels expressed by hippocampal pericytes are functional in resting conditions and mediate a molecular exchange with the cerebral

microenvironment. a Etd*-uptake (arbitrary units) by hippocampal pericytes from global KO Panx1 $^{-/-}$ mice (red; n = 5) is decreased relative to WT mice (black; n = 8); unpaired two-tailed t-test. **b** Fluorescent microphotographs show mimetic peptide 10 Panx1 inhibiting pericyte Etd*-uptake in WT hippocampal slices. **c** Etd*-uptake coefficients of pericytes from WT hippocampal slices are insensitive to Cx blockers, La³+ (n = 5), Gap19 (n = 6), Gap26 (n = 7), and scrambled peptide $^{\text{Scr}}$ Panx1 (n = 5), but respond to Panx1 blockers PBD (n = 5) and 10 Panx1 (n = 5) relative to control (dashed line; n = 8); pericytes from Panx1 $^{-/-}$ KO mice are unresponsive to all blockers, CBX (n = 8), Gap19 (n = 5) and 10 Panx1 (n = 6) compared to its control (n = 8). All data were normalized relative to control WT. Two-tailed one-sample t-test, compared to control WT (over bars); one-way-ANOVA with post-hoc Tukey (over solid lines). **d** Tamoxifen administration to Pdgfrb/Panx1 $^{\text{A/A}}$ and Pdgfrb.CRE-/Panx1 $^{\text{R/B}}$ littermate mice. **e** Etd*-uptake (arbitrary units) by pericytes of hippocampal slices from conditional Pdgfrb/Panx1 $^{\text{A/A}}$ mice (n = 5) is decreased relative to Pdgfrb.CRE-/Panx1 $^{\text{R/B}}$ littermates (n = 5); unpaired two-tailed t-test. **f** The Etd*-uptake coefficient of

pericytes from Pdgfrb.CRE-/Panx1^{fl/fl} slices is inhibited by CBX (n = 6) and ¹⁰Panx1 (n = 5) compared to control (dashed line; n = 6) but remains unresponsive to Gap19 (n = 5). In contrast, dye-uptake by hippocampal pericytes from Pdgfrb/Panx1 $^{\Delta/\Delta}$ mice is insensitive to all blockers, CBX (n = 5), Gap19 (n = 5), and 10 Panx1 (n = 5), compared to its own control (n = 5). All data were normalized relative to control Pdgfrb.CRE-/Panx1^{fl/fl}. Two-tailed one-sample t-test, compared to control Pdgfrb.CRE-/Panx1^{fl/fl} (over bars); one-way-ANOVA with post-hoc Tukey (over solid lines). g Intraperitoneal administration of, vehicle 10 ml/kg and PBD 200 mg/kg to WT mice. h Etd+-uptake (arbitrary units) by hippocampal pericytes from PBDtreated mice (n = 5) decreased compared to vehicle-treated mice (n = 4), unpaired two-tailed t-test. i Etd+-uptake coefficients of hippocampal pericytes after in vivo treatments [Veh (dashed line), n = 4; PBD, n = 5] and ex vivo treatments [Ctrl (dashed line), n = 7: PBD, n = 51, show similar effects. Two-tailed one-sample t-test. PBD compared to vehicle (in vivo) or control (ex vivo) (over bars); unpaired twotailed t-test (between indicated conditions). In (a, c, e, f, h, i), data are presented as mean ± SEM. (n) number of mice. Source data are provided as a Source Data file.

Panx1 in Apy-evoked dilation. We then evaluated the Panx1 involvement in hippocampal capillary responses elicited by exogenous ATP (Fig. 6a, b). After 15 min treatment with ATP (100 µM), capillary diameter near pericyte somata in WT slices decreased (30%) compared to control; narrowing was less pronounced at remote locations, reflecting the impact of pericyte somata on capillary diameter. Suppression of Panx1 in Pdgfrb.Panx1^{△/∆} pericytes abolished ATP-evoked constriction observed in WT slices, implicating pericyte Panx1 in ATP-induced constriction (Fig. 6c-e). Likewise, constriction between pericyte and non-pericyte sites in WT capillaries after ATP treatment was superior compared to control (38%); despite not abolished, ATP-induced narrowing was attenuated in Pdgfrb.Panx1^{∆/∆} mice (12%) confirming pericyte Panx1 participation in ATP-evoked constriction (Fig. 6f-j). We thus hypothesized that ATP released through pericyte Panx1 channels is necessary to achieve a sufficient concentration of ATP near the pericyte somata to constrict capillaries. To test this, we compensated for the lack of Panx1 channels-released ATP in Pdgfrb.Panx1 $^{\Delta/\Delta}$ slices, by applying 10-fold ATP concentration (1 mM). Under these conditions. constriction was restored in Pdgfrb.Panx1^{Δ/Δ} capillaries at pericyte somata (23%, significantly larger compared to constriction under ATP $100 \,\mu\text{M}$; p = 0.044, one-way-ANOVA with post-hoc Tukey) as well as between pericyte and non-pericyte capillary sites (20% increase, significantly larger compared to constriction under ATP 100 μM, $p < 1 \times 10^{-6}$, one-way-ANOVA with post-hoc Tukey) (Fig. 7a-c). Altogether, our data suggest that Panx1 channels provide pericytes an intrinsic mechanism to amplify capillary responses by adjusting local levels of ATP through changes in channel's activity (Fig. 7d).

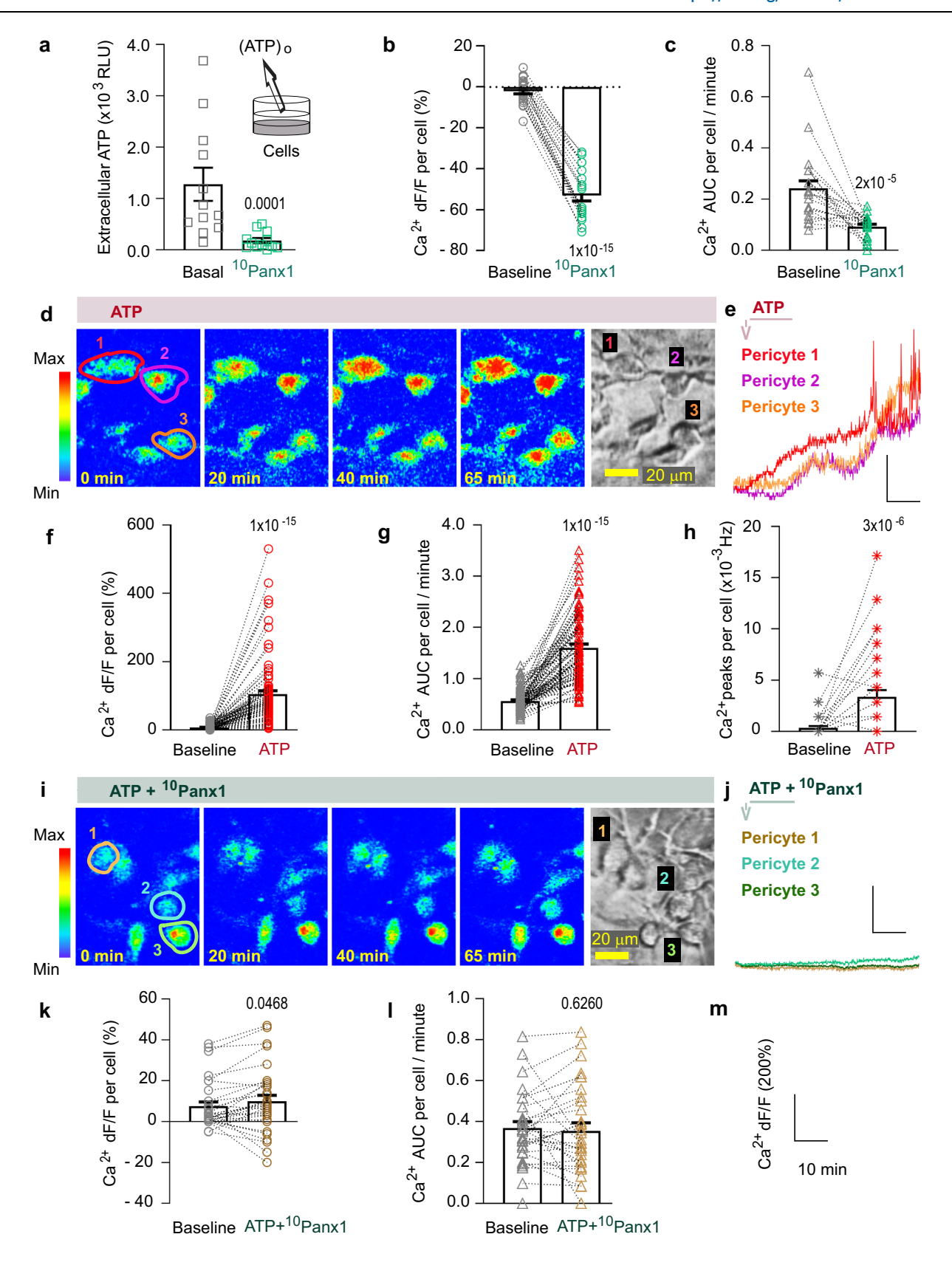
Glutamate inhibits pericyte Panx1 channels activity through ionotropic NMDA/AMPA receptors and dilates hippocampal capillaries through pericyte Panx1

Given that glutamatergic signaling decreases the capillary resistance during functional hyperaemia^{4,56,57} and because glutamate is the brain's main excitatory neurotransmitter and most brain energy expenditure is intended to support synaptic function¹, we hypothesized that glutamate-elicited neurotransmission could correlate with decreases in, pericyte Panx1 channels activity, ATP release and pericyte Ca2+, leading to capillary dilation. To test this, we exposed hippocampal slices to glutamate to mimic neuronal release. Glutamate evoked a dose-dependent reduction (18-68%) in pericyte uptake, with maximum inhibition observed at concentrations exceeding 250 µM, to finally stabilize (Supplementary Fig. 8a). Low Mg²⁺-ACSF did not significantly reduce dye-uptake per se, suggesting that endogenous glutamate does not impact pericyte basal permeability. Since activity-dependent brain hyperaemia is mediated by neuronalderived glutamate acting on post-synaptic α-amino-3-hydroxy-5methyl-4-isoxazolepropionic acid (AMPA) and N-methyl-D-aspartate receptors (NMDA) receptors⁵⁸⁻⁶³, we investigated if AMPAR/NMDAR could also mediate glutamate-evoked pericyte Panx1 channels inhibition. Application of the AMPAR antagonist 6-cyano-7-nitroquinoxaline-2,3-dione (CNQX; 15 μM) or the NMDAR blocker (RS)-3-(2carboxypiperazin-4-yl)-propyl-1-phosphonic acid (CPP; 20 μM) to WT slices in presence of glutamate (500 µM), partially rescued glutamate-evoked uptake inhibition (Glu, 68%; CNQX+Glu, 22%; CPP + Glu, 44%). When applied together, glutamatergic antagonists almost completely recovered pericyte uptake to near control (CNQX + CPP + Glu, 5% inhibition; Supplementary Fig. 8b). Accordingly, single activation of AMPAR (40 µM) or NMDAR (40 µM), respectively, reduced uptake by 46% and 29%, whilst simultaneous activation inhibited uptake by 64%; global knockout of Panx1 abrogated inhibitory effects of glutamatergic signaling implicating Panx1 channels (Supplementary Fig. 8c). Likewise, deletion of Panx1 in pericytes suppressed glutamate-induced dye-uptake inhibition in conditional Pdgfrb/Panx1^{Δ/Δ} mice, confirming the involvement of Panx1 expressed by pericytes (Supplementary Fig. 5). Pericyte cultures were unresponsive to glutamate and AMPAR/NMDAR (Supplementary Fig. 9), in line with previous studies⁶⁴. Thus, glutamate may inhibit pericyte Panx1 activity likely through neuronal postsynaptic NMDA/AMPA receptors, with a major contribution of AMPAR acting on a brain cell type other than pericytes or through a diffusible signaling molecule.

Next, we investigated Panx1 contribution to glutamate-evoked capillary response. Consistent with prior reports $^{4.56}$, 15 min treatment of WT slices with glutamate (500 μ M) increased hippocampal capillary diameter (18%) primarily near pericyte somata. Likewise, glutamate increased capillary diameter between pericyte and non-pericyte sites in WT mice compared to control (by 24.6%). Suppression of Panx1 in Pdgfrb.Panx1 $^{\text{A/A}}$ pericytes inhibited the glutamate-evoked dilation observed in WT mice (Fig. 8a–d), demonstrating that pericyte Panx1 mediates capillary response.

In vivo administration of the Panx1 blocker probenecid induces cerebral capillary dilation

Consistent with our working model, closing pericyte Panx1 channels reduces the pericyte tone, dilating brain capillaries (Fig. 7d). To explore the effect of Panx1 inhibition in freely moving mice, we used the Panx1 inhibitor probenecid. This blocker, with a 2–12-h half-life, inhibits cerebral Panx1 channels when administered in vivo^{38,65} and attenuates Panx1 activity in brain pericytes when applied both in vivo and ex vivo (Fig. 2c, h, i). To induce closure of Panx1 channels in behaving animals, we administered PBD (200 mg/kg, i.p.) to WT and Pdgfrb.Panx1^{Δ/Δ} mice (Fig. 9a), following the same protocol as shown in Fig. 2g. After a 20-min waiting period to allow the drug to take effect, we analyzed vessel diameters in sections of the cortex



and hippocampus. As predicted, closure of Panx1 channels by PBD lead to increased hippocampal and cortical capillary diameters by 20% and 18%, respectively, primarily near pericyte somata, compared to mice injected with the vehicle. Additionally, PBD increased the diameters of hippocampal and cortical capillaries in WT mice, with diameters being larger at pericyte sites relative to non-pericyte

sites (by 18% and 13%, respectively) compared to vehicle-injected mice. Suppression of Panx1 in Pdgfrb.Panx1 $^{\Delta/\Delta}$ pericytes prevented the PBD-evoked dilation observed in WT mice (Fig. 9b–i), demonstrating the role of pericyte Panx1 in mediating the capillary response to PBD in both hippocampal and cortical structures in the intact brain.

Fig. 3 | Panx1 channels mediate ATP release and amplify Ca²⁺ signaling in cultured cerebral pericytes. a Extracellular ATP levels (Relative Luminescence Units-RLU) in pericyte culture media collected under control (12 samples; 4 independent experiments) are decreased under ¹⁰Panx1-treated (12 samples, 4 independent experiments) conditions, two-tailed Mann-Whitney test (compared to basal); symbols represent individual samples. b Maximum amplitude of fluorescence intracellular Ca2+ change in cerebral pericytes [dF/F (%)] under basal and 10Panx1treated conditions (22 pericytes, 6 samples, 3 independent experiments). c Fluorescence intracellular Ca2+ response (area under the curve of dF/F (%) per pericyte per minute; AUC/cell/min) under basal and ¹⁰Panx1-treated conditions (22 pericytes, 6 samples, 3 independent experiments). d Pseudo-colored images of time-lapse variations of fluorescence intracellular Ca2+ in ATP-treated cerebral pericytes (1, 2, and 3; bright field) and e respective Ca²⁺ responses in same pericytes (calibration bars in "m"). f Maximum amplitude of fluorescence intracellular Ca2change in cerebral pericytes [dF/F (%)] under basal and ATP-treated conditions. (94 pericytes, 6 samples, 3 independent experiments). g Fluorescence intracellular Ca24

response (AUC/cell/min) under basal and ATP-treated conditions (90 pericytes, 6 samples, 3 independent experiments). **h** Frequency of Ca²⁺ oscillations [10⁻³ peaks/sec (Hz)] under control and ATP-treated conditions (43 pericytes, 7 samples, 3 independent experiments). **i** Pseudo-colored images illustrate time-lapse variations of fluorescence intracellular Ca²⁺ in ATP plus ¹⁰Panx1-treated cerebral pericytes (1, 2, and 3; bright field) and **j** respective Ca²⁺ responses in same pericytes (calibration bars in "m"). **k** Maximum amplitude of fluorescence intracellular Ca²⁺ change in cerebral pericytes [dF/F (%)] under basal and ATP plus ¹⁰Panx1-treated conditions (32 pericytes, 5 samples, 3 independent experiments). **l** Fluorescence intracellular Ca²⁺ response (AUC/cell/min) under basal and ATP plus ¹⁰Panx1-treated conditions (32 pericytes, 6 samples, 3 independent experiments). **m** Calibration bars used in (**e**, **j**). In (**b**, **l**), paired two-tailed t-test (compared to baseline); in (**c**, **f**, **g**, **h**, **k**), two-tailed Wilcoxon signed-rank test (compared to baseline). In (**b**, **c**, **f**, **g**, **h**, **k**, **l**), symbols represent individual pericytes. In (**a**-**c**, **f**-**h**, **k**, **l**), data are presented as mean ± SEM. Source data are provided as a Source Data file.

Pericyte Panx1 sustains memory function and learningdependent capillary dilation

Given the contribution of pericyte Panx1 to capillary diameter regulation in the hippocampus and cortex (Fig. 9), along with the known involvement of these brain regions in memory function⁶⁶, we hypothesized that disruptions in pericyte Panx1 expression may impair memory performance. To demonstrate so, we conducted novel object recognition and location memory tasks (respectively NOR and OLT) (Fig. 10a, d). The OLT assesses spatial learning and memory, which are dependent on the hippocampus, while the NOR test evaluates nonspatial learning related to object recognition, engaging cortical brain regions⁶⁷. Both the NOR and OLT tasks were impaired in pericyte Panx1-deficient mice (Fig. 10b, c, e, f), suggesting that pericyte Panx1 is required to support healthy cognition, likely by regulating the capillary resistance and blood flow in hippocampus and cortex during brain activity. Accordingly, it has been reported that hippocampus-engaged novel object location and exploration behaviors induce hippocampal microvascular functional hyperaemia, with sustains increases in blood flow that can last up to 1h before returning to baseline⁶⁸. To obtain evidence supporting this possibility, we assessed hippocampal capillary diameters in mouse brain under control conditions (i.e., without undergoing learning and memory tasks) and following OLT in WT animals and mice with deletion of Panx1 in pericytes (Fig. 10g). Consistent with previous reports, mice subjected to OLT showed an increase in hippocampal capillary diameters (15%), primarily near pericyte somata, compared to sham mice. Besides, OLT led to augmented dilation of hippocampal capillaries in WT mice between pericyte and non-pericyte sites relative to non-pericyte sites (by 9% compared to sham mice). Suppression of Panx1 in Pdgfrb.Panx1^{Δ/Δ} pericytes inhibited the OLT-evoked capillary dilation observed in WT mice, demonstrating the role of pericyte Panx1 in mediating the behavior-dependent hemodynamic response (Fig. 10h, i).

Discussion

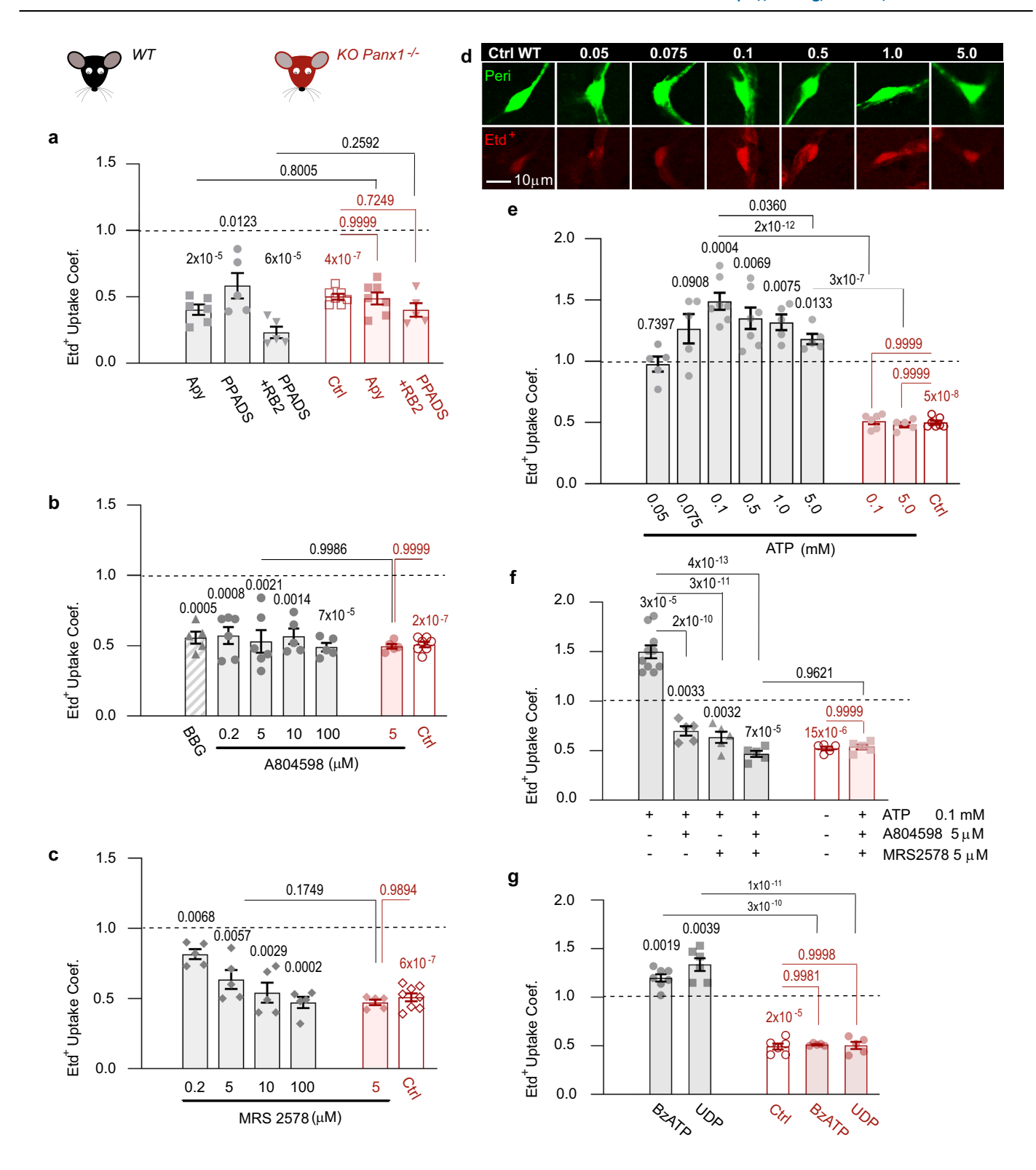
By combining genetic, molecular, functional, and pharmacological approaches, we here uncover the expression of ATP-releasing Panx1 channels in cerebral pericytes, providing direct evidence of their role in regulating the cerebral capillary dynamics and brain function.

We confirmed the molecular identity of Panx1 channels in brain pericytes by demonstrating that pericyte dye-uptake and ATP release are sensitive to Panx1 blockers in WT and Pdgfrb.CRE-/Panx1^{fl/fl} mice. In contrast, pericytes from animals with a genetic deletion of Panx1, global Panx1^{-/-}, and conditional Pdgfrb.Panx1^{Δ/Δ} knockout mice showed no response. Indirect evidence indicated that hippocampal pericyte Panx1 channels are functional in awake, freely moving mice. In this regard, pericyte dye-uptake decreased in probenecid-treated WT mice compared to vehicle-injected controls; similar reductions were observed in global KO Panx1^{-/-} and conditional Pdgfrb.Panx1^{Δ/Δ} mice

compared to respective WT and age-matched littermates lacking the Cre recombinase mice (Fig. 2). Finally, the Panx1 protein was detected in cerebral pericytes (Supplementary Fig. 3).

We demonstrated that the basal activity of pericyte Panx1 channels is sustained by endogenous ATP and is enhanced by exogenous ATP. Pericyte purinergic ionotropic P2X7 and metabotropic P2Y6 receptors, functionally linked to Panx1 channels^{18,50} mediated those effects (Fig. 4, Supplementary Figs. 5-7). We also found that pericyte Panx1 channel activation promotes ATP release (Fig. 3a), which could amplify ATP efflux by activating additional pericyte purinergic receptors and Panx1 channels. This positive feedback mechanism of ATPinduced ATP release may sustain ongoing pericyte ATP outflow through Panx1 channels until reaching an ATP level within the vicinity of the pericyte membrane, as reported in other systems^{45,69}. However, this positive feedback loop would be limited, as higher extracellular ATP concentrations beyond a threshold result in a diminished stimulatory effect on channel activity (Fig. 4d, e). This self-limited regulation earliest described in Panx1-expressing oocytes and likely attributable to direct inhibition of Panx1 or Panx1/P2X7R internalization triggered by high-concentration extracellular ATP would prevent deleterious actions of exacerbated ATP accumulation70-74. Besides P2X7R and P2Y6R, other purinergic receptor subtypes may also be activated by the Panx1-mediated ATP release.

In addition to pericyte Panx1 channel activity, extracellular ATP fluctuations regulated hippocampal capillary diameter through pericyte Panx1; decreased endogenous ATP led to vessel dilation, whereas increased extracellular ATP through exogenous application caused vessel contraction (Figs. 5 and 6). How would pericyte Panx1 channels mediate those vascular effects? While we cannot rule out that ATP upregulates acto-myosin function through P2X7R/Panx175, ATP constricts capillaries by increasing intracellular Ca²⁺, which enhances the pericyte tone and resistance to capillary blood flow^{3,23,27,28}. Local variations in neuronal activity or vasoactive signals could enhance or reduce pericyte Panx1 activity, leading to either an increase or decrease in the continuous release of ATP from pericytes, respectively promoting constriction or dilation of adjacent capillaries (Fig. 7). This view is supported by several results, (a) pharmacological silencing of pericyte Panx1 channels inhibited ATP release and ATP-evoked Ca2+ signaling (Fig. 3), (b) pericyte deletion of Panx1 abrogated Apy-induced capillary dilation and inhibited ATP-evoked constriction (Figs. 5 and 6), and (c) increasing exogenous ATP restored ATP-evoked capillary constriction in conditional Pdgfrb.Panx1^{Δ/Δ} mice (Fig. 7). Consistent with the idea that pericyte Panx1 channels regulate extracellular ATP levels nearby the pericyte membrane to enhance the dynamic range of pericyte/capillary functionality, previous studies have correlated Panx1 expression in SMCs with vessel behavior. In resistance arteries, α₁-adrenergic receptor-mediated vasoconstriction involves the activation of Panx1 in SMCs and subsequent purinergic signaling. Using



pharmacological and genetic approaches, the Isakson group demonstrated that Panx1 expression levels in SMCs regulate the extent of vasoconstriction and the blood pressure response to sympathetic stimulation; thus, the expression of Panx1 channels in SMCs potentiates vasoconstriction and blood pressure⁷⁶. These effects depend, at least in part, on ATP release through Panx1 channels^{26,76,77}.

In pericytes, vasoactive agents other than ATP may be released through Panx1 channels, while mechanisms independent of Panx1's channel properties could affect pericyte contractility through different pathways. For instance, Rho-kinase-dependent inhibition of actin depolymerization enhances brain pericytes´ tone¹6. The possibility of Panx1 interacting with Rho-GTPases to control actin polymerization was recently reported in CA1 hippocampal neurons⁷⁸. Further research will be necessary to decipher all these aspects in brain pericytes.

Interestingly, glutamate-evoked capillary dilation required pericyte Panx1 (Fig. 8). Given that glutamatergic-mediated neurotransmission plays a key role in CBF increase in response to cerebral activity^{4,56,57,60,79}, this finding discloses the potential relevance of pericyte Panx1 channels in functional in vivo hyperaemia under those circumstances. The lumen diameter is a primary factor influencing the

Fig. 4 | Extracellular ATP fluctuations regulate pericyte Panx1 channels' activity in mouse hippocampal slices through purinergic ionotropic P2X7 and metabotropic P2Y6 receptors. a Etd+-uptake coefficients of hippocampal pericytes from WT (black) mice decrease by apyrase (Apy; n = 6) and purinergic blockers, PPADS (n = 5) and PPADS + RB2 (n = 5) compared to control (dashed line; n = 9); pericytes from global KO Panx1^{-/-} (red) mice are unresponsive (Ctrl, n = 7; Apy, n = 7; PPADS + RB2, n = 5). **b** Etd⁺-uptake coefficients of WT pericytes decrease with purinergic P2X7 blockers BBG (n = 5) and A804598 (0.2 μ M, n = 6; 5 μ M, n = 6; 10 μ M, n = 5 and 100 μ M, n = 5) compared to control (dashed line; n = 7); pericytes from global KO Panx1^{-/-} mice are unresponsive (Ctrl, n = 7; A804598, n = 5). c Etd⁺uptake coefficients of WT pericytes decrease with purinergic P2Y6 blocker MRS2578 (0.2 μ M, n = 5; 5 μ M, n = 5; 10 μ M, n = 5 and 100 μ M, n = 5) compared to control (dashed line: n = 5): pericytes from global KO Panx1^{-/-} mice are unresponsive (Ctrl, n = 8; MRS2578, n = 5). d Fluorescent images depict Etd⁺-uptake by WT pericytes under control and ATP-treated conditions. e Etd+-uptake coefficients of WT pericytes augment with increasing doses of ATP (0.05 mM, n = 5; 0.075 mM,

n = 5; 0.1 mM, n = 7; 0.5 mM, n = 7; 1 mM, n = 5; 5 mM, n = 5) compared to control (dashed line; n = 7); Etd*-uptake coefficients of ATP-treated pericytes from KO $Panx1^{-/-}$ mice remain unchanged compared to control KO (Ctrl. n = 7: ATP. 0.1 mM. n = 6; 5 mM, n = 5). **f** Etd⁺-uptake coefficients of WT pericytes treated with ATP (0.1 mM) decrease with purinergic P2X7 and P2Y6 blockers A804598 and MRS2578 (ATP, n = 10; ATP + A804598, n = 5; ATP + MRS2578, n = 5; ATP + A804598 + MRS2578, n = 5) compared to ATP alone and to control (dashed line; n = 10); dyeuptake by pericytes from global KO Panx1^{-/-} mice remain unchanged compared to control KO (Ctrl, n = 5; ATP + A804598 + MRS2578, n = 5). g Etd+-uptake coefficients of WT pericytes increase with BzATP (n=7) or UDP (n=6) compared to control (dashed line; n = 7); dye-uptake by pericytes from global KO Panx1^{-/-} mice remain unchanged (Ctrl, n = 6; BzATP, n = 5; UDP, n = 5). In (a-c, e-g), two-tailed onesample t-test, compared to control WT (over bars); one-way-ANOVA with post-hoc Tukey, between indicated conditions (solid lines). All data were normalized relative to control WT. In $(\mathbf{a}-\mathbf{c}, \mathbf{e}-\mathbf{g})$, data are presented as mean \pm SEM. (n) number of mice. Source data are provided as a Source Data file.

vascular resistance to blood flow; according to Poiseuille's law, resistance is inversely proportional to the fourth power of the vessel's radius. Then, based on our data, we estimate that glutamatergic transmission could rise hippocampal capillary blood flow by ~94-144%, if measured at the pericyte sites. How might Panx1 facilitate capillary dilation triggered by glutamatergic transmission? Inhibition of pericyte Panx1 channels by glutamate and the resulting decrease in local ATP release and pericyte Ca²⁺ (Figs. 3 and 7d and Supplementary Fig. 8) is one potential scenario. Dye-uptake by cultured cerebral pericytes was insensitive to glutamatergic agonists (Supplementary Fig. 9). Consistently, prior studies reported that cerebral microvascular pericytes are resistant to glutamatergic stimuli⁶⁴. Thus, glutamatergic effects on pericyte Panx1 channels in hippocampal slices could involve a cell type distinct from pericytes. How could pericyte Panx1 react to the micro-environmental glutamate? It is well established that neuronal AMPAR/NMDA-evoked glutamatergic synaptic transmission induces messengers' release from neuro-glial origin, which relaxes pericytes. Among those messengers, nitric oxide and arachidonic acid (and its metabolites) play a major role in capillary dilation^{4,7}. Therefore, the release of these vasodilators during activation of glutamatergic NMDA/AMPA receptors could eventually inhibit pericyte Panx1 channels as elsewhere 80,81, leading to capillary dilation. In neurons, glutamatergic NMDA receptors activate Panx1 channels during synaptic plasticity⁸², anoxia/ischemia⁸³, and epileptiform seizure activity⁸⁴. The release of signaling molecules (e.g., ATP, adenosine) through open neuronal Panx1 channels upon NMDA receptor activation could also influence pericyte tone under both physiological and pathological conditions. Furthermore, redox changes associated with local metabolic variations resulting from glutamatergic synaptic activity could potentially modulate pericyte Panx1 channels properties85.

Consistent with our working model (Fig. 7d), pharmacological closure of Panx1 channels with probenecid in behaving mice led to capillary dilation in both the hippocampus and cortex, an effect abolished in conditional Pdgfrb/Panx1 $^{\Delta/\Delta}$ mice (Fig. 9), confirming that Panx1 modulates cerebral capillary diameter via its channel activity. Importantly, our approach to evaluating the impact of in vivo pericyte Panx1 channel closure on brain capillary diameters relied on lowimpact procedures. This minimized the influence of surgical trauma and systemic anesthesia, both of which are known to affect channel and expression⁸⁶⁻⁸⁸. Although probenecid phenylephrine-induced contraction of the thoracic aorta⁸⁹, its dilatory effect on cerebral capillaries is largely unexplored. Originally prescribed for gout treatment, probenecid has recently gained attention as a pharmacological agent for various central nervous system disorders, including cerebral ischemic injury. Currently, its neuroprotective effects are primarily attributed to its anti-inflammatory properties linked to Panx1 inhibition38,90-92.

Mechanisms regulating the CBF are crucial for proper brain function. Cerebral capillary hyperaemia may involve increased blood flow to meet metabolic demands of active neurons during tasks such as learning, memory, or sensory processing. Pericytes are principal elements in the neurovascular responses underlying cognition^{93,94}. In this regard, we demonstrated that pericyte Panx1 supports memory performance and maintains cerebral capillary dilation during learning and memory (Fig. 10), providing substantial conceptual insight into the neurovascular interface, as opposed to the traditional neurocentric explanation of the mechanisms underlying these functions⁹⁵⁻⁹⁷. Specifically, we propose that the impairments in NOR and OLT performance observed in conditional pericyte Panx1 mice (Fig. 10a-f) are associated with disrupted capillary diameter regulation in the cortex and hippocampus, respectively (Fig. 9), likely due to the capillary system's inability to supply sufficient metabolic resources to meet neuronal demands during activity. Accordingly, genetic deletion of pericyte Panx1 blunted capillary widening following OLT (Fig. 10g-i). How could pericyte Panx1 sense neuronal activity under these circumstances? As mentioned before, the release of diffusible dilators nitric oxide and arachidonic acid of neuro-glial origin during cerebral activity and synaptic glutamatergic transmission is one possibility; these brain messengers might inhibit pericyte Panx1 channels, leading to capillary dilation^{4,7,80,81}. Finally, given the association between cognitive deficiency and dysfunctional pericytes98,99, our findings establish a framework for understanding cognitive disorders associated with cerebrovascular diseases, focusing on the neurovascular unit, with Panx1 channels as a target.

In summary, the metabolic exchange between blood and brain occurs at cerebral capillaries, which serve as primary source of energy supply and main contributors of cerebrovascular resistance and CBF. Our study establishes pericyte Panx1 as a regulator of cerebral capillary diameter that sustains memory, and describes a mechanism at the basis of this function. Future research aimed at identifying neuronal mediators targeting pericyte Panx1 during learning and memory, as well as exploring the role of pericyte Panx1 in cerebrovascular pathologies, will strengthen our understanding of the mechanisms feeding the brain in health and disease.

Methods

Animals

Experimental procedures were conducted in accordance with the National Institutes of Health guidelines for the care and use of Laboratory animals (NIH Publications No. 8023, revised 1978) and the local regulation [CDC Exp. 4332/99, Diario Oficial No. 25467, Feb. 21/00, Universidad de la República, Uruguay]. The Committee on Animal Research Ethics (Law 18.611) (Facultad de Medicina—Udelar) approved

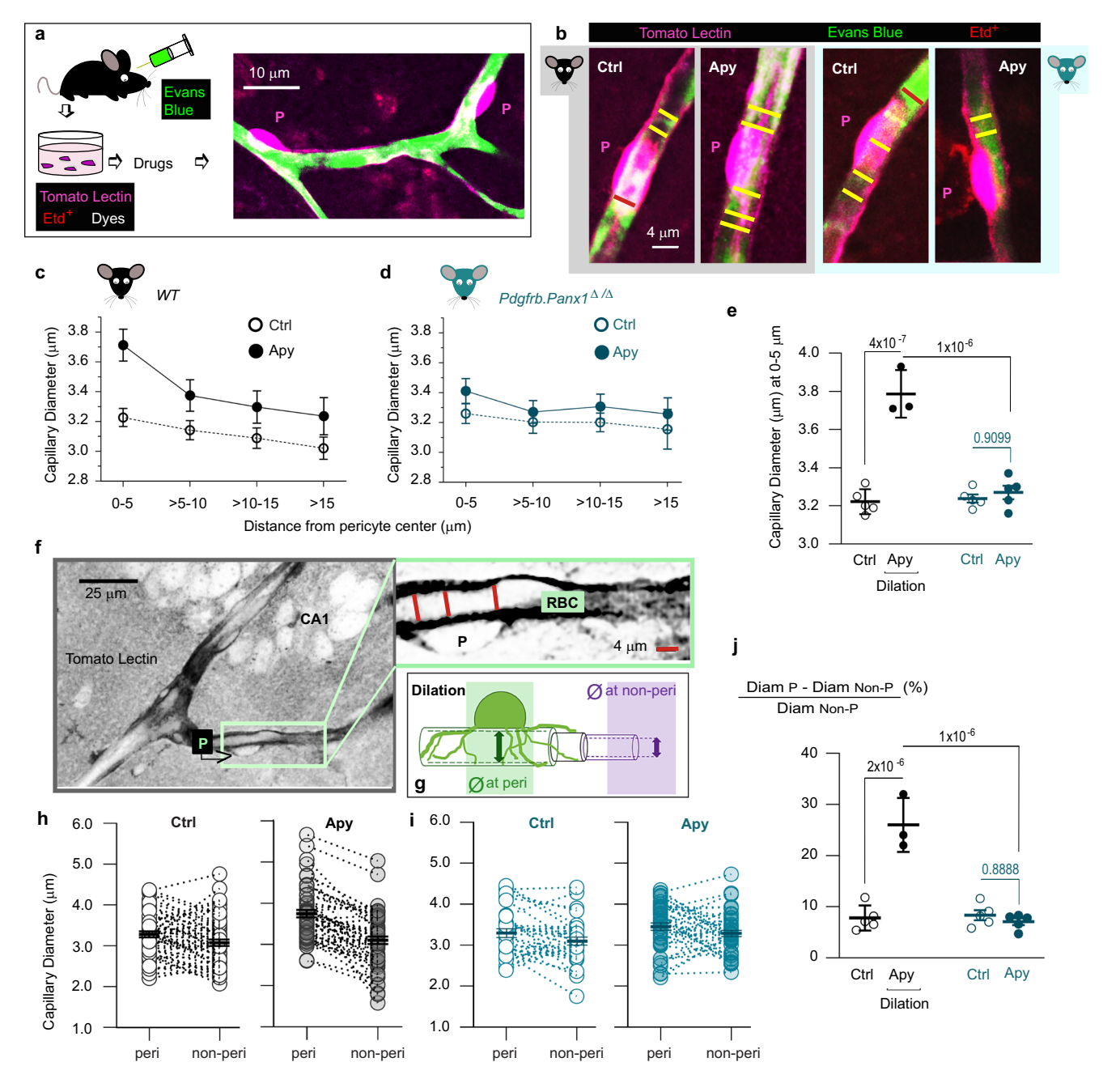


Fig. 5 | **Deletion of Panx1 in pericytes abrogates apyrase-associated capillary dilation in hippocampal slices. a** (left) Staining procedure labeling of cerebral pericytes and vasculature with fluorescent dyes (Evans Blue; Tomato-Lectin-DyLight 488; Etd*); (right) Fluorescently labeled vessels and pericytes (P) in a mouse hippocampal slice. **b** Fluorescent images of capillaries and pericyte somas (P) in resting (Ctrl) and apyrase-treated (Apy; 8 U/ml) hippocampal slices from WT (black) and Pdgfrb/Panx1^{Δ/Δ} (blue-green) mice; yellow and red lines exemplify measurements of internal vessel diameters. Capillary diameter (μm) as a function of distance from pericyte somata in hippocampal slices from WT (**c**; Ctrl, n = 5; Apy, n = 3) and Pdgfrb/Panx1^{Δ/Δ} (**d**; Ctrl, n = 5; Apy, n = 5) mice in resting (Ctrl) and Apytreated conditions. For illustrative purposes, capillaries from all mice were pooled and averaged. **e** Capillary diameter (μm) at (0–5 μm) from pericyte somata in control and Apy-treated hippocampal slices from WT (Ctrl, n = 5; Apy, n = 3) and Pdgfrb/Panx1^{Δ/Δ} (Ctrl, n = 5; Apy, n = 5) mice. **f** Tomato-Lectin-labeled vessels and

pericyte (P) in a hippocampal slice; in zoomed green box, red lines show measurements of internal vessel diameters; RBC, red blood cells. **g** Illustration of diameter measurements at pericyte and non-pericyte sites of capillaries during dilation. Individual diameter values (μ m) obtained at pericyte and non-pericyte zones of each analyzed vessel (paired symbols) under control and Apy-treated hippocampal slices derived from WT (**h**; Ctrl, n = 5; Apy, n = 3) and Pdgfrb/Panx1^{A/A} (**i**; Ctrl, n = 5; Apy, n = 5) mice; mean diameter values (μ m) obtained at pericyte/non-pericyte zones have been overlaid. **j** Percentage of capillary diameter change between pericyte and non-pericyte zones normalized to non-pericyte zone (%) in control and Apy-treated hippocampal slices from WT (Ctrl, n = 5; Apy, n = 3) and Pdgfrb/Panx1^{A/A} (Ctrl, n = 5; Apy, n = 5) mice. In (**e**, **j**), one-way ANOVA with post-hoc Tukey, between indicated conditions. In (**c**, **d**, **e**, **j**), data are presented as mean \pm SEM. (n) number of mice. Source data are provided as a Source Data file.

the protocols (protocol numbers: 070153-000740-17, 070153-000045-19, and 070153-000109-19).

Male and female rats (Sprague Dawley; P14-P30) were employed for cultures, and wild-type (WT) and global knockout pannexin1 (KO Panx1^{-/-}) mice (Mus musculus; P21-P31) on a C57BL/6 background¹⁰⁰

for dye-uptake experiments. Global KO Panx1^{-/-} mice derived from heterozygous Panx1^{-/-} embryos that were generously gifted by Genentech Corporation (Genentech, Inc., South San Francisco, CA 94080), cryo-recovered and bred as a homozygous colony by the Laboratory Animal Biotechnology Unit (Institut Pasteur de

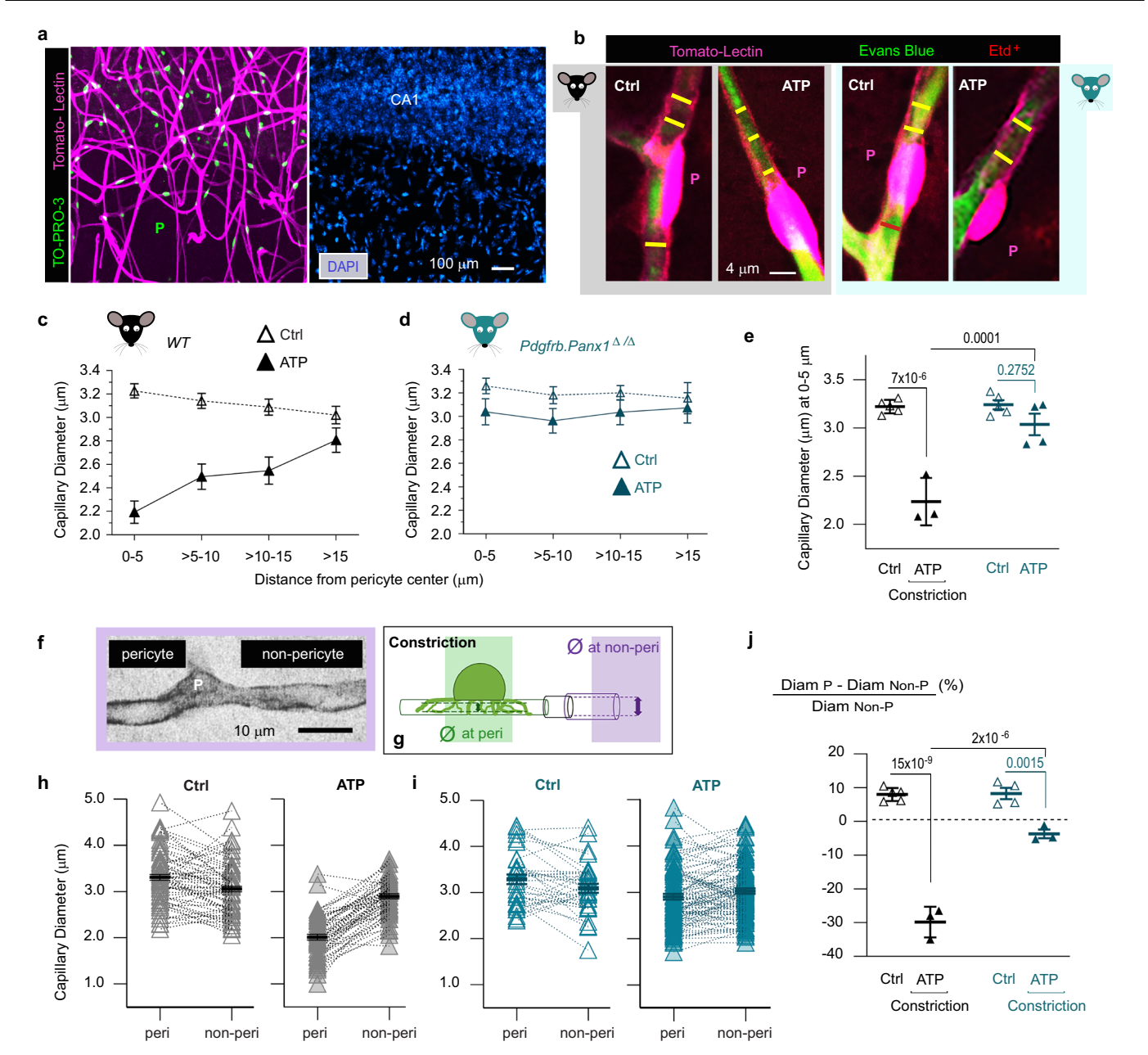


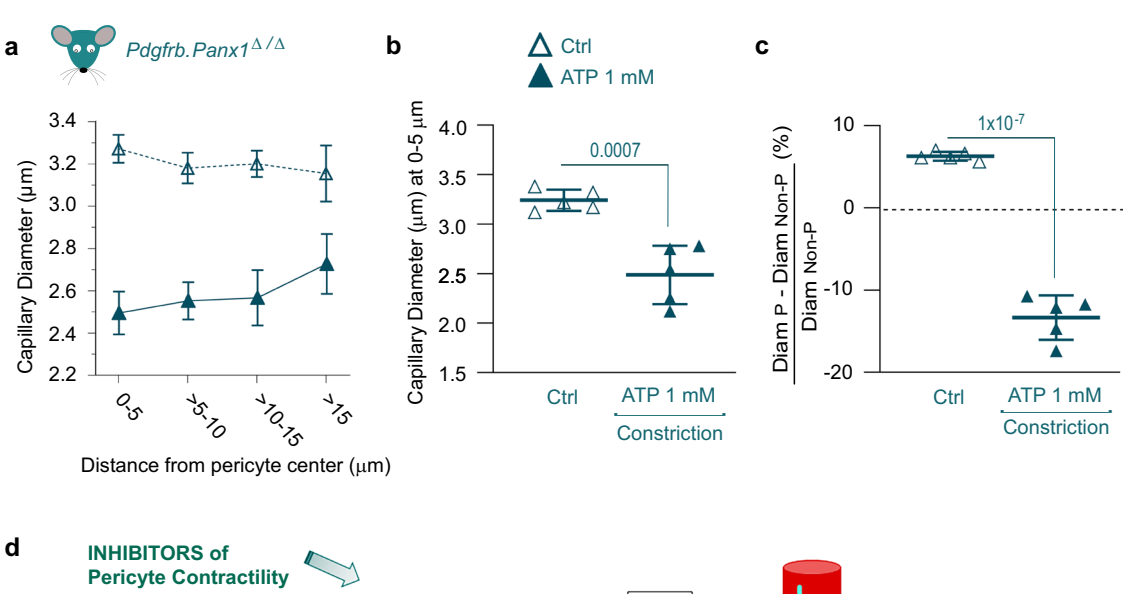
Fig. 6 | **Deletion of Panx1 in pericytes attenuates ATP-induced capillary constriction in hippocampal slices. a** Representative views from the *stratum radiatum* and CA1 region of a mouse hippocampal slice show labeled vessels and pericytes (P); both images are from the same field. **b** Representative fluorescent capillaries and pericyte somas (P) in resting conditions (Ctrl) and after superfused ATP (100 μM) in hippocampal slices derived from WT (black) and Pdgfrb/Panx1 $^{A/\Delta}$ (blue-green) mice; yellow and red lines illustrate measurements of internal vessel diameters. Capillary diameter (μm) as a function of distance from pericyte somata in hippocampal slices derived from WT (**c**; Ctrl, n = 5; ATP, n = 3) and Pdgfrb/Panx1 $^{A/\Delta}$ (**d**; Ctrl, n = 5; ATP, n = 4) mice in resting conditions and after superfused ATP. For illustrative purposes, capillaries from all mice were pooled and averaged. **e** Capillary diameter (μm) at (0–5 μm) from pericyte somata in control and ATP-treated hippocampal slices derived from WT (Ctrl, n = 5; ATP, n = 3) and

Pdgfrb/Panx1^{A/A} (Ctrl, n = 5; ATP, n = 4) mice. **f** Tomato-Lectin-labeled vessel and pericyte (P) in hippocampus. **g** Illustration of diameter measurements at pericyte and non-pericyte sites of capillaries during constriction. Individual diameter values (μ m) obtained at pericyte and non-pericyte sites of each analyzed vessel (paired symbols) in control and ATP-treated (100 μ M) conditions in hippocampal slices derived from WT (**h**; Ctrl, n = 5; ATP, n = 3) and Pdgfrb/Panx1^{A/A} (**i**; Ctrl, n = 4; ATP, n = 3) mice; mean diameter values (μ m) obtained at pericyte/non-pericyte zones have been overlaid. **j** Percentage of capillary diameter change between pericyte and non-pericyte sites normalized to non-pericyte zone (%) in control and ATP-treated hippocampal slices derived from WT (Ctrl, n = 5; ATP, n = 3) and Pdgfrb/Panx1^{A/A} (Ctrl, n = 4; ATP, n = 3) mice. In (**e**, **j**), one-way ANOVA with post-hoc Tukey, between indicated conditions. In (**c**, **d**, **e**, **j**), data are presented as mean ± SEM. (n) number of mice. Source data are provided as a Source Data file.

Montevideo—Uruguay). The absence of Panx1 gene was determined by genotyping.

To evaluate the role of pericyte Panx1 in vascular functionality and cognition, mice with deletion of Panx1 in pericytes (Pdgfrb/Panx1^{Δ/Δ}) were genetically engineered by crossing Panx1^{R/R} floxed mice carrying *loxP* sites flanking exon 3–4 of the pannexin1 gene (The Jackson Laboratory; Strain #026021, B6;129-Casp4^{del} Panx1^{tmlVshe}/J)¹⁰¹ with mice

expressing tamoxifen-sensitive cre-ER^{T2} recombinase driven by the murine platelet-derived growth factor receptor beta polypeptide (Pdgfrb) promoter (The Jackson Laboratory; Strain # 030201, B6.Cg-Pdgfrb^{tml.1/cre/ERT2/Csln}/J)¹⁰². Since the latter strain was bred in heterozygosis, crossings produced offspring with and without Pdgfrb-Cre/ERT2. The Panx1^{fl/fl} floxed littermate driven by Pdgfrb and lacking the Cre recombinase (Pdgfrb.Cre-/Panx1^{fl/fl}), as well as the WT mice, were



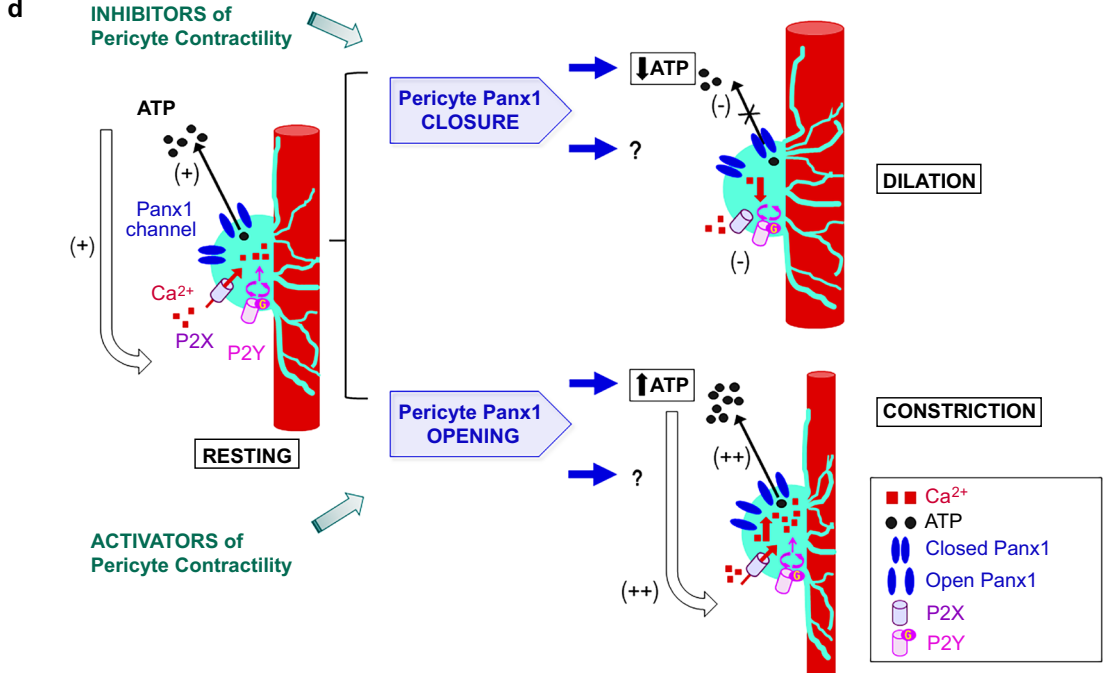


Fig. 7 \mid Increased superfused ATP restores ATP-dependent capillary constriction in hippocampal slices derived from pericyte Panx1-deficient mice.

a Capillary diameter (μ m) as a function of distance from pericyte somata in hippocampal slices derived from Pdgfrb/Panx1^{A/A} mice (blue-green) under resting conditions (Ctrl, n = 5) and after superfused ATP (1 mM, n = 5). For illustrative purposes, capillaries from all mice were pooled and averaged. **b** Capillary diameter (μ m) at (0–5 μ m) from pericyte somata in control (Ctrl, n = 5) and ATP-treated (ATP, n = 5) hippocampal slices derived from Pdgfrb/Panx1^{A/A} mice. **c** Percentage of capillary diameter change between pericyte and non-pericyte sites normalized to non-pericyte zone (%) in control (Ctrl; n = 5) and ATP-treated (ATP 1 mM, n = 5) hippocampal slices derived from Pdgfrb/Panx1^{A/A} mice. In (**b**, **c**), unpaired two-tailed t-test, between indicated conditions. In (**a–c**), data are presented as mean \pm SEM. (n) number of mice. **d** Proposed working model of pericyte Panx1-mediated

intrinsic mechanism regulating cerebral capillary dynamics. In "resting" brain areas, a certain number of open Panx1 channels at pericyte membrane mediates tonic release of ATP contributing to set basal intracellular Ca²+ and pericyte contractility through ionotropic P2X7 and metabotropic P2Y6 purinergic receptors. Inhibitors of pericyte tone would switch off this mechanism by closing Panx1 channels, favoring pericyte relaxation, capillary dilation, and subsequent increase in cerebral blood flow at that level. Conversely, in presence of stimulators of pericyte tone, an enhanced number of active pericyte Panx1 channels would amplify local ATP release, pericyte intracellular Ca²+, and contractility, leading to capillary constriction and decreased local cerebral blood flow. Other diffusible compounds released through pericyte Panx1 channels, as well as additional purinergic receptor subtypes, might also contribute to regulating cerebral capillary diameter. Source data are provided as a Source Data file.

used as controls. Conditional pericyte Panx1-deleted mice and control littermates were generated by the Laboratory Animal Biotechnology Unit (Institut Pasteur de Montevideo—Uruguay). The presence/ absence of Pdgfrb-CRE/ERT2 gene was determined by polymerase chain reaction (PCR).

Animal husbandry

All animals were group-housed in temperature-controlled rooms (21.5 °C; relative humidity 55–70%) on a 12 h light/dark cycle, with food

and water available *ad libitum* at the Unidad de Reactivos y Biomodelos de Experimentación (URBE—Facultad de Medicina).

Tamoxifen-inducible Cre recombinase activation

The expression of Cre recombinase and resultant inactivation of Panx1 in pericytes was induced by tamoxifen¹⁰². Both conditional Pdgfrb/Panx1 $^{\Delta/\Delta}$ and control littermate Pdgfrb.CRE-/Panx1 $^{R/R}$ mice received intraperitoneal (i.p.) injection of tamoxifen (TMX; 2 mg/kg i.p) dissolved in corn oil, 1 dose per 5 consecutive days (at P21–P25).

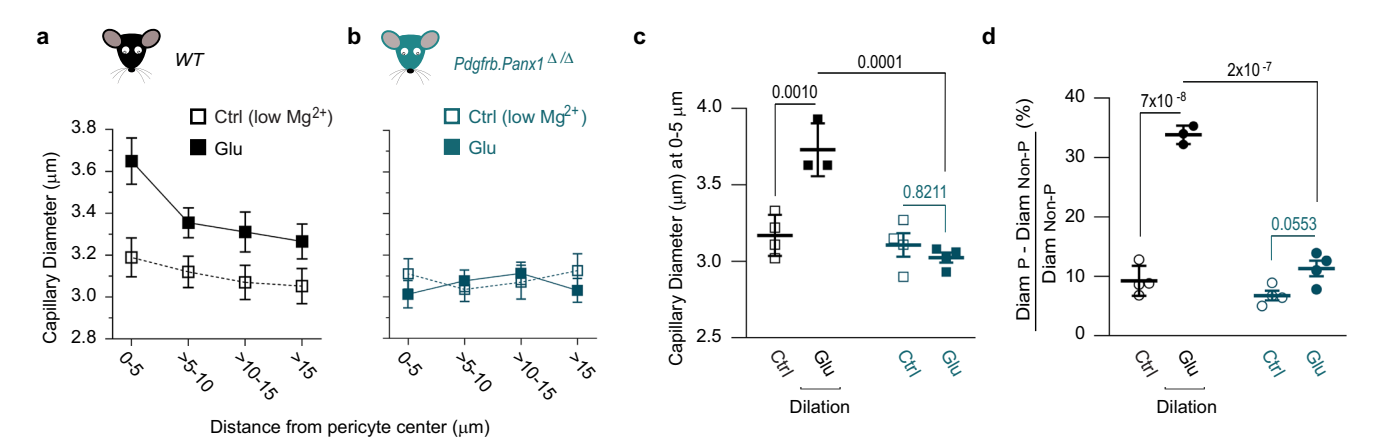


Fig. 8 | **Deletion of Panx1 in pericytes inhibits glutamate-associated capillary dilation in hippocampal slices.** Capillary diameter (μm) as a function of distance from pericyte somata in hippocampal slices derived from WT (**a**; Ctrl, n = 4; Glu, n = 3) and conditional Pdgfrb/Panx1^{Δ/Δ} (**b**; Ctrl, n = 4; Glu, n = 4) mice in resting conditions (Ctrl) and after superfused glutamate (Glu; 500 μM) (WT, black; Pdgfrb/Panx1^{Δ/Δ}, blue-green). For illustrative purposes, capillaries from all mice were pooled and averaged. **c** Capillary diameter (μm) at (0–5 μm) from pericyte somata in control and glutamate-treated hippocampal slices from WT (Ctrl, n = 4; Glu,

n=3) and Pdgfrb/Panx1 $^{\Delta/\Delta}$ (Ctrl, n=4; Glu, n=4) mice. **d** Percentage of capillary diameter change between pericyte and non-pericyte sites normalized to non-pericyte zone (%) in control and glutamate-treated hippocampal slices from WT (Ctrl, n=4; Glu, n=3) and Pdgfrb/Panx1 $^{\Delta/\Delta}$ (Ctrl, n=4; Glu, n=4) mice. In (**c**, **d**), oneway ANOVA with post-hoc Tukey, between indicated conditions. In (**a**–**d**), data are presented as mean \pm SEM. (n) number of mice. Source data are provided as a Source Data file.

Experimental maneuvers were performed on days 5–8 after the last injection (Fig. 2d). Subsequent to TMX administration, the ablation of Panx1 protein was confirmed by immune-techniques (Supplementary Fig. 3), whilst lack of pericyte Panx1 channel's function was evaluated by dye-uptake functional experiments (Fig. 2e, f; Supplementary Fig. 5).

Assessment of Panx1 deletion

The efficiency and specificity of Panx1 deletion in pericytes were validated through expression and functional studies. In WT and control Pdgfrb.CRE-/Panx1^{fl/fl} mice, Panx1 was present in pericytes, vSMCs, endothelium, and neurons, while in global KO Panx1^{-/-} mice, Panx1 was decreased in all cell types. In conditional Pdgfrb/Panx1^{\(\Delta\)} mice. Panx1 was deleted in the majority of pericytes but was present in most vascular smooth muscle cells (vSMCs), endothelium, and neurons within the hippocampus (Supplementary Figs. 3 and 4). Accordingly, treatment of hippocampal slices with ATP (0.1 mM) increased Panx1 channels activity in pericytes and vSMCs from WT mice but not from global KO Panx1^{-/-} mice, whereas in conditional Pdgfrb/Panx1^{Δ/Δ} the effect of ATP on Panx1 channels activity was only suppressed in pericytes but not in vSMCs (Fig. 4, Supplementary Figs. 4 and 5). Finally, vSMCs exhibited basal activity of Panx1 channels, which was reduced in global Panx1 KO (Panx1^{-/-}) mice but not in conditional Pdgfrb/Panx1^{Δ/Δ} mice (Supplementary Fig. 4). Altogether, these findings indicate that Panx1 deletion in conditional Pdgfrb/Panx1^{\(\Delta\)} mice was largely efficient and specific to brain pericytes.

Hippocampal/Cerebral acute slices

To obtain acute transverse hippocampal slices, mice were sacrificed by cervical dislocation and decapitated. Then, hippocampi were dissected and placed in ice-cold artificial cerebrospinal fluid (ACSF) containing (in mM): NaCl 134; KCl 2.8; NaHCO $_3$ 29; NaH $_2$ PO $_4$ 1.1; glucose 12; MgSO $_4$ 1.5; CaCl $_2$ 2.5. Transverse hippocampal slices (200–300 μ m thick) were cut using a vibroslicer and transferred to a storage chamber where they rested on a nylon mesh, submerged in ACSF at room temperature (RT) for a stabilization period of 45 min before use. The ACSF solution was equilibrated with a mixture of 95% O $_2$ and 5% CO $_2$ (pH 7.4). In another set of experiments, coronal cerebral slices (300–400 μ m thick) including the hippocampi and somatosensory cortex were obtained.

Cerebral Pericyte Cultures

To prepare primary cultures of cerebral pericytes³⁹, brains from 3-4week-old rats were rapidly extracted and olfactory bulbs, cerebellum, medulla, and meninges removed. After that, the brain was minced and incubated (1 h; 37 °C) in DMEM containing collagenase I (0.225 mg/ml), CaCl₂ (5 mM), and DNase I (40 µg/mL). Then, the digested tissue was homogenized manually and filtered (80-µm mesh). The homogenate was mixed with a BSA-solution (1.7 volumes of 22% bovine serum albumin) and centrifuged (800 × g; 15 min). The pellet was resuspended (DMEM with 10% FBS), and isolated brain microvessels fragments were seeded on 35-mm Petri dishes pre-coated with collagen I (5 µg/cm²). After reaching confluency (7–8 days), cells were detached (0.05% trypsin-EDTA, 5 min), centrifuged (200 × g, 10 min). and plated on uncovered Petri dishes at 1:3 dilutions in supplemented DMEM. After reaching confluency, a second passage was done and cells were seeded at a density of 10,000-14,000 cells/cm² on cover glass and maintained until confluency (-1 week) to be used in experiments.

Pericyte Identification

In cerebral slices, pericytes were identified with the far-red fluorophore TO-PRO™-3 Iodide 642/661 (ThermoFisher Scientific), which is selectively captured by living pericytes through an active transporter³⁰. Acute hippocampal slices were incubated (20 min) in ACSF (O₂ 95%, CO₂ 5%) containing TO-PRO™-3 (1 μM, RT) protected from light. Then, slices were washed in ACSF (15 min); after washing, TO-PRO™-3-loaded slices were ready to use. Capillary pericytes labeled with TO-PRO™-3 were definitely evident in living and fixed slices¹⁰³. The TO-PRO™-3 staining was visualized in the far-red spectrum (642/661), which allowed multiple-labeling with fluorescent probes such as ethidium bromide (3.8-diamino-5 ethyl-6phenylphenanthridinium bromide) (528/598) and Lycopersicon Esculentum (Tomato) Lectin conjugated to DyLight 488 (493/518) (ThermoFisher Scientific) that were used for dye-uptake and vessel diameter measurements. Additionally, pericyte somas were labeled with Tomato Lectin (see detailed procedure in vessel labeling and diameter evaluation item). In primary cultures, cerebral pericytes were identified by immunofluorescence detection of the neuron-glial antigen 2 (NG2), a chondroitin sulfate proteoglycan, and platelet-derived growth factor receptor beta (PDGFRB) (see

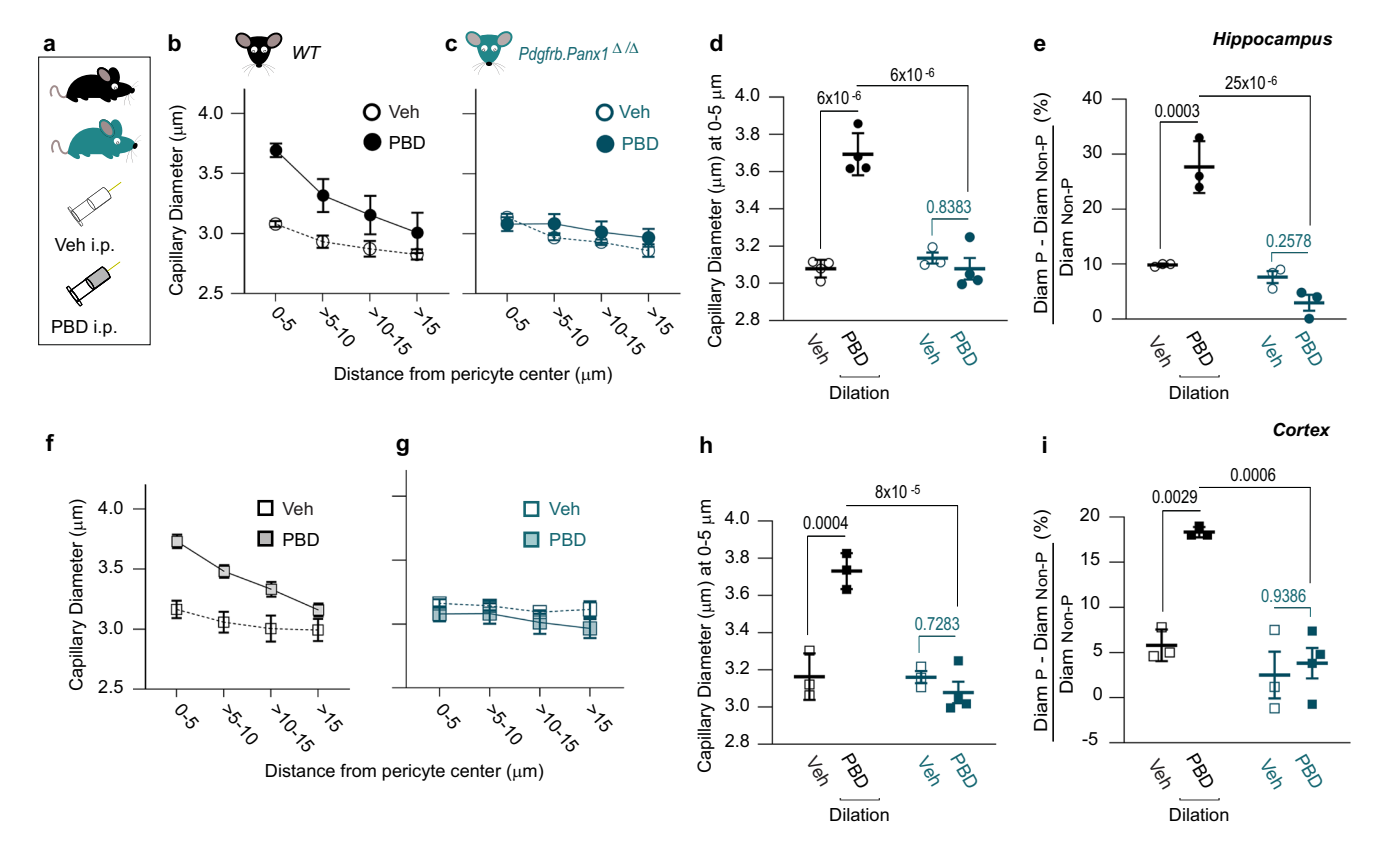


Fig. 9 | Pharmacological inhibition of Panx1 channels by probenecid (PBD) in behaving mice induces cerebral capillary dilation, an effect that is suppressed in pericyte Panx1-deficient mice. a Scheme of intraperitoneal administration of vehicle (Veh; 10 ml/kg) and probenecid (PBD; 200 mg/kg) in WT (black) and conditional Pdgfrb/Panx1^{\Delta/\Delta} (blue-green) mice. Capillary diameter (μ m) as a function of distance from pericyte somata in the hippocampus of WT (b; Veh, n = 4; PBD, n = 4) and Pdgfrb/Panx1^{\Delta/\Delta} (c; Veh, n = 3; PBD, n = 4) mice under resting (Veh) and PBD-treated conditions. d Capillary diameter (μ m) within (0–5 μ m) of pericyte somata in the hippocampus of WT (Veh, n = 4; PBD, n = 4) and Pdgfrb/Panx1^{\Delta/\Delta} (Veh, n = 3; PBD, n = 4) mice. e Percentage of capillary diameter change between pericyte and non-pericyte sites normalized to non-pericyte zone (%) in the hippocampus of WT

(Veh, n = 3; PBD, n = 3) and Pdgfrb/Panx1^{Δ/Δ} (Veh, n = 3; PBD, n = 3) mice. Capillary diameter (μm) as a function of distance from pericyte somata in the cortex of WT (\mathbf{f} ; Veh, n = 3; PBD, n = 3) and Pdgfrb/Panx1^{Δ/Δ} (\mathbf{g} ; Veh, n = 3; PBD, n = 4) mice under resting (Veh) and PBD-treated conditions. \mathbf{h} Capillary diameter (μm) within (0–5 μm) of pericyte somata in the cortex of WT (Veh, n = 3; PBD, n = 3) and Pdgfrb/Panx1^{Δ/Δ} (Veh, n = 3; PBD, n = 4) mice. \mathbf{i} Percentage of capillary diameter change between pericyte and non-pericyte sites normalized to non-pericyte zone (%) in the cortex of WT (Veh, n = 3; PBD, n = 3) and Pdgfrb/Panx1^{Δ/Δ} (Veh, n = 3; PBD, n = 4) mice. In (\mathbf{d} , \mathbf{e} , \mathbf{h} , \mathbf{i}), one-way ANOVA with post-hoc Tukey, between indicated conditions. In (\mathbf{b} - \mathbf{i}), data are presented as mean \pm SEM. (n) number of mice. Source data are provided as a Source Data file.

immunofluorescence section). Most cultured pericytes (PDGFR β -positive) expressed α SMA but not PDGFR α (Supplementary Fig. 1), suggesting pericyte contractile functions without strong association with the PDGFR α -marked fibroblast population. It must be noted that the high percentage of α SMA-expressing pericytes in culture may not be representative of the thin-strand pericytes in situ.

Immunofluorescence

To prevent non-specific binding and facilitate membrane permeabilization, fixed preparations were immersed in a multiwell dish in agitation for 2 h in blocking solution, which consisted of 2% bovine serum albumin (BSA) and 0.2 M glycine diluted in PBS with 0.5% Triton X-100 (PBST). After three washes with PBST, slices were incubated for at least 24 h at 4 °C in PBST containing 2% BSA (PBST-BSA) along with one of the following primary antibodies: mouse monoclonal anti-NG2 chondroitin sulfate proteoglycan (Millipore #MAB5384, 1:250); mouse monoclonal platelet-derived growth factor receptor beta or PDGFR\$ (Abcam. #ab69506, 1:50); rabbit polyclonal PDGFRα (Abcam. #ab61219, 1:150); rabbit polyclonal alpha-smooth muscle actin or αSMA (Abcam. #ab5694, 1:100); rabbit polyclonal anti-Panx1 (Sigma-Aldrich #HPA016930, 1:40), rabbit polyclonal anti-Panx1 (Alomone Labs. #ACC-234, 1:200), rabbit polyclonal anti-P2X7R (Alomone Labs. #APR-004, 1:200), rabbit polyclonal anti-P2Y6R (Alomone Labs. #APR-011, 1:500), rabbit monoclonal anti-NeuN (Abcam #Ab177487, 1:200),

or rabbit monoclonal anti-GFAP-Cy3TM (Sigma-Aldrich #C9205, 1:400). Afterward, the slices underwent two rinses in PBST and were placed in dark for 2 h in a secondary antibody [Alexa Fluo 488 anti-rabbit or antimouse, Alexa Fluo Cy3 anti-rabbit or anti-mouse (Jackson Labs., #711-545-152, #715-545-151, #111-165-003, #115-165-003; 1:1000)] that was diluted in the same medium. Subsequent to three washes (10 min in PBST), slices were incubated with DAPI (1–5 μ M diluted in PBST; 10 min) and then rinsed once again. Finally, slices were mounted in glycerol and examined using a confocal laser-scanning microscope (Leica SP5 TANDEM SCANNER). Confocal images were captured utilizing appropriate lasers and the LAS AF Software in xyz data mode. The omission of primary antibodies did not yield any positive staining in any of the trials.

Western blotting

To detect Panx1 in cerebral pericytes, primary cultures of rat brain pericytes were processed for Western blotting analysis. To do so, fresh samples were collected and sonicated in tissue lysis buffer containing 50 mM NaCl, 50 mM HEPES, 2 mM sodium orthovanadate, 1% Triton X-100, and SigmaFAST Protease inhibitor cocktail (Sigma-Aldrich). After protein quantification and denaturation, 40 µg of protein samples was seeded in a 12% SDS-PAGE gel and then transferred to a nitrocellulose membrane. The membranes were first incubated for 1 h in blocking solution (5% BSA in 0.1% Tween-PBS) and then overnight at 4 °C with

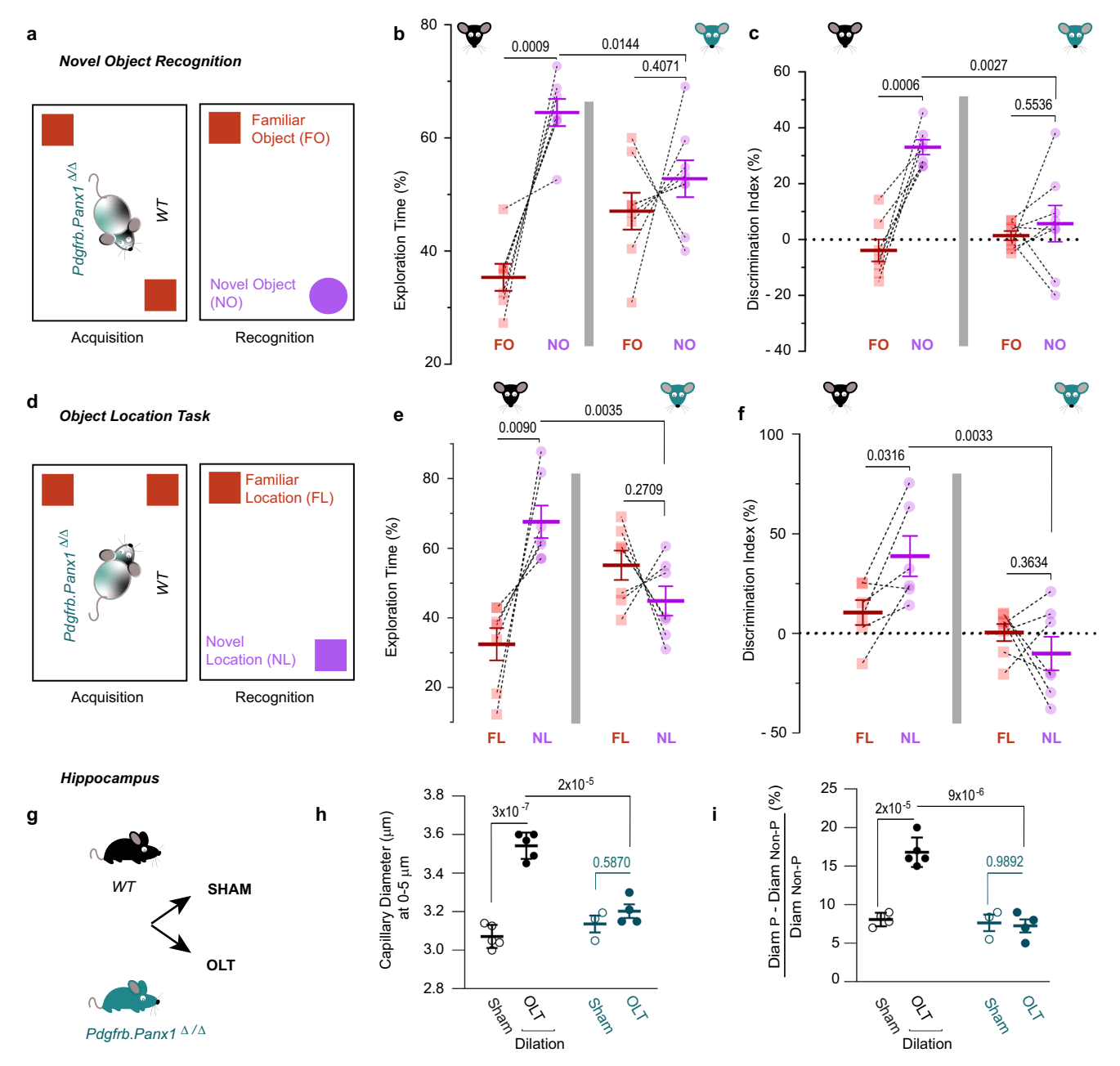


Fig. 10 | **Pericyte Panx1 is required for object recognition (NOR) and location (OLT) memory and learning-evoked capillary dilation.** a Scheme of novel object recognition test (NOR test) procedure conducted in WT (black) and conditional Pdgfrb/Panx1 $^{\Delta/\Delta}$ (blue-green) mice. **b** Percentage of exploration time (%) for familiar (FO; red) and novel (NO; violet) objects in WT (n = 7) and Pdgfrb/Panx1 $^{\Delta/\Delta}$ (n = 8) mice. **c** Discrimination Index (%) between familiar (FO) or between familiar and novel (NO) objects in WT (n = 7) and Pdgfrb/Panx1 $^{\Delta/\Delta}$ (n = 8) mice. **d** Scheme of novel object location test (OLT) procedure. **e** Percentage of exploration time (%) for familiar (FL; red) and novel (NL; violet) locations in WT (n = 7) and Pdgfrb/Panx1 $^{\Delta/\Delta}$ (n = 7) mice. **f** Discrimination Index (%) between familiar (FL) or between familiar and novel (NL) locations in WT (n = 6) and Pdgfrb/Panx1 $^{\Delta/\Delta}$ (n = 7) mice. In (**b**, **c**, **e**, **f**):

paired two-tailed t-test, between FO and NO groups and between FL and NL groups, and unpaired t-test, between groups from different mouse strains. **g** Scheme of mice groups used for the study. **h** Capillary diameter (μ m) within (0–5 μ m) of pericyte somata in the hippocampus of WT (Sham, n=5; OLT, n=5) and Pdgfrb/Panx1^{Δ/Δ} (Sham, n=3; OLT, n=4) mice. **i** Percentage of capillary diameter change between pericyte and non-pericyte sites normalized to non-pericyte zone (%) in the hippocampus of WT (Sham, n=4; OLT, n=5) and Pdgfrb/Panx1^{Δ/Δ} (Sham, n=3; OLT, n=4) mice. In (**h**, **i**), one-way ANOVA with post-hoc Tukey, between indicated conditions. In (**b**, **c**, **e**, **f**, **h**, **i**), data are presented as mean ± SEM. (n) number of mice. Source data are provided as a Source Data file.

anti-Panx1 antibody (1:400; Sigma-Aldrich #HPA016930) together with anti-βactin antibody (1:400; Sigma-Aldrich #A5441) that was used as a protein loading control. Afterward, the membranes were washed and incubated for 1h at room temperature with IRDye 680RD/IRDye 800CW-conjugated Goat Anti-Mouse IgG and Goat Anti-Rabbit IgG secondary antibodies (1:15000 in PBS each, LI-COR Biosciences #926-68070, #926-32211). Western blot images were acquired using the

Odyssey CLx imaging system and analyzed with Image Studio software (version 2.0; LI-COR Biosciences).

Ethidium uptake assays

In ex vivo hippocampal slices. The activity of pericyte Panx1 channels was assessed by ethidium bromide (3.8-diamino-5 ethyl-6-phenylphenanthridinium bromide) (Etd⁺, 314 Da) permeability assay

in acute brain slices as reported¹⁰⁴. This relatively large molecule permeates large-pore channels present at cell membranes; once intracellular. Etd+ binds irreversibly to nucleic acids and fluoresce. For this, acute hippocampal slices were incubated (20–30 min) in ethidium bromide containing ACSF (Etd*-ACSF) solution equilibrated with 95% O₂, 5% CO₂ (pH 7.4 at RT). The Etd⁺-ACSF solution was prepared from a 10 mM stock solution of Etd⁺ dissolved in PBS and applied to ACSF at 10 µM final concentration. Drugs (blockers, transmitters, vasoactive agents) were added to the Etd+-ACSF solution. Treatments with glutamate and its agonists/antagonists were conducted in low Mg2+-ACSF solution to allow NMDA receptor activation and lasted a maximum of 15 min to prevent NMDA-dependent neurotoxicity. Low Mg²⁺-ACSF contained (in mM): NaCl 135; KCl 2.8; NaHCO₃ 29; NaH₂PO₄ 1.1; glucose 12; MgSO₄ 0.5; CaCl₂ 2.5. Following recordings with Etd⁺, slices from control and test groups were rinsed (15 min) in normal ACSF to stop dye-uptake, remove unbound Etd+, and reduce background labeling. After, slices were fixed (4% PFA in PBS; 40 min), rinsed twice (PBS; 10 min), counterstained with DAPI (1 µM in PBST; 10 min) under mild shaking and protected from light, rinsed once again and mounted in glycerol until photographs were taken. At 4 °C, Etd⁺ labeling was stable for ~1-2 months.

In cultured brain pericytes (in vitro). Pericyte cultures were incubated in culture medium containing 10 μ M Etd⁺ (at 5% CO₂, 37 °C, 20 min). Following dye-uptake recordings, cultures were washed several times in PBS to stop uptake, and subsequently fixed with 4% PFA (30 min, RT). Drugs were applied 5 min prior, and during Etd⁺ recordings. Finally, cells were mounted with glycerol-PBS containing Hoechst 33342 (1 μ g/ml).

After in vivo manipulation of Panx1 channels. To evidence the functionality of pericyte Panx1 channels in resting conditions, the Panx1 blocker probenecid (PBD; 200 mg/kg weight dissolved in physiological solution) was injected (i.p.) to the test group and the vehicle to the sham group. In all cases, the vehicle volume was adjusted to 10-12 μL/g weight. Then, animals were restored to their cages, where they stayed in a quiet environment. Following 20 min, mice were sacrificed, hippocampi dissected, and slices acutely obtained (Fig. 2g). Acute hippocampal slices were loaded with TO-PRO™-3 to label pericytes and incubated (20 min) in Etd+-ACSF solution equilibrated with 95% O2, 5% CO2 (pH 7.4 at RT) as described before in "In ex vivo hippocampal slices." After, sections were fixed (PFA 4%; 40 min), labeled with DAPI (1-5 μM), mounted in mounting media (glycerol), and analyzed through confocal microscopy. Mice employed in these studies did not show signs of suffering (i.e., freezing, aggression, presence of stereotyped movements, changes in exploratory behavior, increased defecation, respiratory distress) during the 20 min following the beginning of the treatment with vehicle or PBD until the animal's sacrifice.

Vessel labeling for diameter assessment

For vessel labeling during ex vivo treatments, TO-PRO $^{\text{TM}}$ -3-loaded slices were incubated at 37 °C (15 min) with Lycopersicon Esculentum (Tomato) Lectin conjugated to DyLight 488 (Tomato-Lectin; 5 µg/ml) a fluorescent probe that binds to glycosylated residues in basement membranes of pericytes and endothelium resulting in visualization of vessel contours and pericyte somas $^{33,105-107}$. To evidence vessel internal boundaries, the fluorescent dye Evans Blue (470-540/680) was administered into the intravascular space, where the probe is retained due to its high affinity to serum albumin, which does not permeate healthy cell membranes. For this, prior to slice obtaining, mice were anesthetized with isoflurane (4–5%) with an inhalation anesthesia equipment (VETEQUIP Impac 6). Then, Evans Blue (EB; 6 mg dissolved in 100 μ L of physiological solution) was applied by retro-orbital injection of the venous sinus in the eye retrobulbar space with a 0.5-in insulin needle¹⁰⁸.

After recovery, mice were sacrificed for slice preparation and dye loading (with TO-PRO™-3, Etd⁺, Tomato Lectin). Acute dye-loaded slices were then treated (for 15-20 min) with one of these drugs, i.e., glutamate (500 μM), Apy (8 U/ml), or ATP (100 μM and 1 mM) and, subsequently, fixed (PFA, 4%; 40 min). Importantly, animals were not systemically perfused with fixing solution to avoid perturbing vessel diameters during systemic perfusion. In a set of experiments, acute slices were placed on the bottom of a perfusion chamber for living experiments as reported³0,10³. Nuclei from fixed and living slices were respectively counterstained with 2-[4-(Aminoiminomethyl) phenyl] −1*H*-Indole-6-carboximidamide hydrochloride (DAPI; 1–5 μM in PBST; 10 min) or Hoechst 33342 (0.5 μM in PBST; 10 min) at RT under gentle shaking.

For capillary diameter assessment following in vivo treatments, the Panx1 blocker probenecid (PBD; 200 mg/kg weight dissolved in physiological solution) was injected (i.p.) to the test group and the vehicle to the sham group as described [see "Inhibition of Panx1 channels in the freely behaving mice" in the "Ethidium Uptake Assays" section]. Then, animals were restored to their cages, where they stayed in a quiet environment. Following 20 min, mice were sacrificed, brain removed, and acute cerebral slices rapidly obtained and fixed (PFA, 4%; 40 min). After, fixed slices were incubated with Tomato-Lectin conjugated to DyLight 488 (1:500 in PBST; 2 h; RT) under smooth shaking and protected from light. Then, sections were rinsed (3×; 10 min in PBS), incubated with DAPI (1–5 μ M diluted in PBST; 15 min), and then rinsed once again. For capillary diameter assessment following the object location recognition task (OLT), brains from both sham mice and those engaged in the behavioral task were removed and subjected to the same procedure. Fixed slices were mounted in mounting medium (glycerol) and kept at 4°C protected from light before image acquisition. Images of either fixed (offline acquisition) or living (online acquisition) slices were then taken (see image acquisition section).

Viability cell assessment

We assessed hippocampal cell viability in slices using ethidium homodimer-1 (EthD-1, 857 Da; Life Technologies), a cell-impermeant dye that labels damaged/dead cells with disrupted membranes and not solely those undergoing programmed cell death. Slices were incubated with EthD-1 (200 nM, 15 min, RT), rinsed (20 min), fixed (PFA 4% in PBS, 40 min), and mounted for imaging. No dead cells were detected beyond $10\text{--}20\,\mu\text{m}$ from the slice surface.

Image acquisition in fixed and living slices

Fixed tissue sections were placed onto the platform of a confocal microscope (Leica SP5 TANDEM SCANNER). Acute loaded slices were secured at the base of a homemade flow-through chamber, perfused with ACSF (1 ml/min; 95% O₂ and 5% CO₂), and mounted onto the confocal microscope. Labeled cells were observed using a 40x oil immersion objective, Leica N.A 1.3, with UV correction and a 63x oil immersion objective, Leica N.A 1.42, with UV correction. Image stacks were captured with the LAS AF Lite Software in the xyz data mode and sequentially acquired at 1024×1024 pixels/airy resolution through appropriate lasers for DAPI (UV 405 nm), Tomato Lectin (Ar 488 nm), Etd⁺ (HeNe 543 nm), and TO-PRO™-3 (HeNe 633 nm). Gain and offset were adjusted within a range where the signal-to-noise ratio was optimized and there was no saturation of Etd⁺-uptake. Microscope and camera settings were the same in those experiments in which comparisons had to be made. For capillary diameter measurements, photos by differential interference contrast (DIC) microscopy were also captured through an additional channel. Images were acquired at distances greater than 15 µm and not beyond 90 µm from slice surface. We took this approach to exclude damaged cells located either at superficial zones, or in hypo-perfused deep regions where nutrients, gases, drugs and dyes have difficulty accessing and might exhibit irregular propagation across the slice depth^{4,33,103,109,110}. Capillaries were

identified by their small diameter ($<10\,\mu m$), absence of smooth muscle cells, and presence of pericytes. Healthy capillaries were selected according to reported criteria³³.

Dye-uptake quantification

Dve-uptake, measured as intracellular Etd+ fluorescence intensity. reflects the number of active Panx1 channels present at the cell membrane. Pericyte dye-uptake was assessed with the Image I software (NIH, Bethesda, MD, USA). The contours of TO-PRO™-3-labeled pericyte somas were manually outlined in the TO-PRO™-3 channel, and the fluorescence intensity of the selected somas (ROIs) was measured in the Etd+ channel. The fluorescence intensity of the intracellular Etd+ was quantified in arbitrary units as the difference $(F-F_0)$ between the fluorescence (F) measured at pericyte somas and the background fluorescence (F₀) measured in areas of the same field devoid of cells. We typically averaged the dye-uptake of 3 to 6 pericytes from 4 to 6 fields of view across 4 to 6 slices per condition per mouse. Then, we normalized Etd+ fluorescence averages of treated conditions to untreated (control) condition. To quantify dye-uptake by cultured pericytes, a similar procedure was followed by quantifying the fluorescence intensity in fields of pericyte monolayers.

Capillary diameter measurements

To analyze capillary diameters, vessels with clearly delineated walls and pericytes with fusiform somas in the mid-capillary zones were selected. The internal capillary calibers are more sensitive to vasomodulators and experimental conditions than external ones. Thus, internal diameters were manually measured by drawing a line within the vessel lumen perpendicular to the longitudinal vessel axe at distances close (<5 µm) or far (>5 µm) from the pericyte soma, by using the Image J software (Windows 32-bit; National Institutes of Health, NIH, Bethesda, MD, USA)^{33,39}. Lines extended between inner limits of vascular walls photographed in the same focal plane. Results were represented as the diameter change relative to the pericyte distance (in um) as reported⁵⁴ or as the percentage of diameter change at the pericyte sites in comparison to the non-pericyte sites of vessels (%). To calculate the last parameter, the difference (in µm) between the diameters measured at both pericyte and non-pericyte zones of analyzed capillaries was divided by the diameter at the nonpericyte zone (in µm), which is believed to be less influenced by the pericyte tone^{54,55}. We typically analyzed one or two capillary diameters per slice in ex vivo treatments and averaged the diameters of 15 to 47 capillaries per mouse for in vivo treatments. In slices, caliber measurements from vessels imaged using either DIC or fluorescence were similar. Likewise, capillary diameters measured in fixed and live hippocampal slices were consistent (Supplementary Fig. 10). Notably, hippocampal capillary diameters at pericyte somata in both liveimaged and fixed WT slices were comparable to those reported in previous studies16,111.

Extracellular ATP quantification

The levels of extracellular ATP were measured in cultured cerebral pericytes through the luciferin-luciferase bioluminescence assay (Invitrogen™; cat. A22066). To do this, a second passage of primary pericyte cultures were seeded on a 4-well plate at a density of 25,000 cells/well. After 7 DIV, cells were treated with 150 µM ¹ºPanx1 or vehicle (DMSO) for 24 h before ATP determination. The standard luciferin-luciferase solution was prepared according to the company's protocol and introduced into a 96-well plate, where three samples of the media of each condition (control; ¹ºPanx1) were applied to individual wells. Luminescence was measured using a LumiStar Galaxy luminometer and software (BMG Labtech); values were then averaged and quantified as Relative Luminescence Units (RLU). The background level was determined by averaging the luminescence in two wells containing the standard solution and two wells containing supplemented NB medium.

Finally, this background signal was subtracted from the luminescence values of both treated and control samples.

Calcium imaging in brain pericytes

Variations in intracellular calcium levels were assessed in cultured cerebral pericytes previously loaded with the non-ratiometric fluorescent calcium indicator Fluo4-acetoxymethyl ester (Fluo4/AM; ThermoFisher Scientific). To do so, confluent cultured cerebral pericytes in a 4 chamber 35 mm glass bottom dish (Cellvis) were incubated with DMEM containing Fluo4/AM (10 µM; for 40 min at 37 °C in darkness). Any excess indicator was subsequently removed through a washing step (5 min). The glass bottom dishes containing the cell cultures were placed in a chamber (One Stage Top, Okololab) connected to Okolab temperature, gas and humidity controllers (37 °C and 5% CO₂) and mounted onto the stage of a confocal microscope (Leica SP5 TANDEM SCANNER) equipped with filters for Fluo4 (excitation/emission 488/ 515 nm). Labeled cells were observed with a 63x oil immersion objective, Leica N.A 1.3, with UV correction. Time-lapse variations of Fluo4/ AM fluorescence were acquired at 0.14 Hz in cerebral pericytes (ROIs) using the LAS AF Lite Software through laser Ar 488 nm. In all cases, light bright-field photos of pericytes were taken. Drugs (150 µM ¹⁰Panx1; 100 μM ATP) were applied to cells following 10 min baseline registration. Recordings lasted 20-40 min maximum and were analyzed using the Image J software (NIH, Bethesda, MD, USA). Results were represented as dF/F (%) = $(F_t-F)/F$, in which F_t depicted the fluorescence generated during the experimental condition, and F represented the baseline fluorescence in recorded pericytes (ROIs) obtained by averaging initial (5-10 min) fluorescence signals. Additionally, the area under the curve (AUC) was also calculated for pericytes (ROIs) in time-lapse Fluo4/AM fluorescence recordings by using the Image J software (NIH, Bethesda, MD, USA) and was represented per minute of recording.

Behavioral testing: novel object recognition and object location memory tasks

The novel object recognition (NOR) and object location (OLT) tasks were developed according to earlier publications with minor modifications^{67,112,113}. One week prior to testing, animals were handled for 1 min during 5 consecutive days by the same experimenter to prevent manipulation-induced stress. On trial day, mice were acclimatized to the testing room for 30 min minimum before the test's initiation (pre-habituation). The tests were conducted during the light phase of the 12 h light/dark within a single day and comprised a habituation period followed by two trials. On habituation period, each mouse was introduced (10 min) into an empty arena (without objects) consisting on a polypropylene box for unrestricted exploration [NOR: 32 cm (length) × 22 cm (width) × 23 cm (height)] or [OLT: 44 cm (length) × 31 cm (width) × 21 cm (height)]. After, the mouse was removed from the empty arena and placed into an individual cage (30 min). During each training or acquisition trial, each mouse was placed in an arena with two identical, familiar objects (FO; cubes) fixed to the base and positioned more than 5 cm apart in familiar locations (FL). Following the training period (10 min), the mouse was removed from the arena and returned to a clean cage for a 60 min inter-trial interval. On the re-exposure, each mouse was reintroduced (10 min) into the center of the arena where one familiar object or location was replaced by, respectively, a novel object (NO; cylindrical tower) or location (NL) (Fig. 10a, d). Between trials, arena and objects were cleaned with 70 % ethanol and dried. Sham animals (see Fig. 10) were handled like OLT mice and placed in an object-free testing arena, but did not undergo learning and memory tasks. Explorations and interactions with objects were video-recorded. Object exploration was computed as the time periods when the mouse directed its nose towards the object within distances shorter than 2 cm while looking at, sniffing, or touching it. The percentage of exploration time was

calculated as the ratio of the interaction time with the familiar or novel object or location to the total exploration time. The discrimination index was determined as the ratio of the difference in exploration time between the novel object/location and the familiar object/location to the total exploration time (time with novel location or object–time with familiar location or object/time with novel location or object + time with familiar location or object).

Reagents

Otherwise stated, drugs, probes, and salts used in this study were from Sigma-Aldrich. AMPA was from Research Biochemicals International (RBI), and probenecid was acquired from ThermoFisher Scientific. Mimetic peptides Gap26 (VCYDKSFPISHVR), Gap19 (KQIEIKKFK), ¹⁰Panx1 (WRQAAFVDSY), and Scrambled ^{Scr}Panx1 (FADRYWAQVS) were synthesized by Genscript (purity > 95%).

Statistics

Otherwise stated, data are presented as mean ± standard error of the mean (mean ± SEM). No pre-established exclusion criteria were applied; animals were randomly assigned. A minimum of 3 animals per trial was employed. The normality distribution of the sample was assessed through a normality test prior to executing a statistical test. Parametric tests were used for data with a normal distribution, while non-parametric tests were applied to data that did not meet this criterion. Statistical significance of data was determined by one-sample ttest, unpaired t-test, paired t-test, one-way ANOVA followed by Tukey post-test, Wilcoxon matched pairs test, and Mann-Whitney test. All tests were two-tailed. The level of significance was set at p < 0.05. The GraphPad InStat (version 3.06) and GraphPad Prism (version 8.0.2) software (GraphPad Software, San Diego, CA, USA) were used for statistical analysis and graph generation. Figures were prepared with Adobe Photoshop CS6 (version 13.0, 64-bit) and Adobe Illustrator CS6 (version 16.0.0), both from Adobe Inc., San Jose, CA, USA. Symbols in graphs represent individual mice unless specified. Detailed statistical parameters and tests are given in figures and figure legends.

Reporting summary

Further information on research design is available in the Nature Portfolio Reporting Summary linked to this article.

Data availability

All relevant data generated in this study are available in the main text and the Supplementary Information. Source data are provided with this paper.

References

- Harris, J. J., Jolivet, R. & Attwell, D. Synaptic energy use and supply. Neuron 75, 762–777 (2012).
- Roy, C. S. & Sherrington, C. S. On the regulation of the bloodsupply of the brain. J. Physiol. 11, 85–158 (1890).
- Peppiatt, C. M., Howarth, C., Mobbs, P. & Attwell, D. Bidirectional control of CNS capillary diameter by pericytes. *Nature* 443, 700–704 (2006).
- 4. Hall, C. N. et al. Capillary pericytes regulate cerebral blood flow in health and disease. *Nature* **508**, 55–60 (2014).
- Hill, R. A. et al. Regional blood flow in the normal and ischemic brain is controlled by arteriolar smooth muscle cell contractility and not by capillary pericytes. *Neuron* 87, 95–110 (2015).
- Fernández-Klett, F. & Priller, J. Diverse functions of pericytes in cerebral blood flow regulation and ischemia. J. Cereb. Blood Flow. Metab. 35, 883–887 (2015).
- Mishra, A. et al. Astrocytes mediate neurovascular signaling to capillary pericytes but not to arterioles. *Nat. Neurosci.* 19, 1619–1627 (2016).

- Kisler, K. et al. Pericyte degeneration leads to neuro-vascular uncoupling and limits oxygen supply to brain. *Nat. Neurosci.* 20, 406–416 (2017).
- Gould, I. G., Tsai, P., Kleinfeld, D. & Linninger, A. The capillary bed offers the largest hemodynamic resistance to the cortical blood supply. J. Cereb. Blood Flow. Metab. 37, 52–68 (2017).
- Erdener, ŞE., Küreli, G. & Dalkara, T. Contractile apparatus in CNS capillary pericytes. *Neurophotonics* 9, 021904 (2022).
- Wu, D. M., Kawamura, H., Sakagami, K., Kobayashi, M. & Puro, D. G. Cholinergic regulation of pericyte-containing retinal microvessels. Am. J. Physiol. Heart Circ. Physiol. 284, H2083–H2090 (2003).
- 12. Kamouchi, M. et al. Calcium influx pathways in rat CNS pericytes. Brain Res. Mol. Brain Res. 126, 114–120 (2004).
- Puro, D. G. Physiology and pathobiology of the pericytecontaining retinal microvasculature: new developments. *Micro*circulation 14, 1–10 (2007).
- Hamilton, N. B., Attwell, D. & Hall, C. N. Pericyte-mediated regulation of capillary diameter: a component of neurovascular coupling in health and disease. Front. Neuroenergetics 2, 5 (2010).
- Borysova, L., Wray, S., Eisner, D. A. & Burdyga, T. How calcium signals in myocytes and pericytes are integrated across in situ microvascular networks and control microvascular tone. *Cell Calcium* 54, 163–174 (2013).
- Hartmann, D. A. et al. Brain capillary pericytes exert a substantial but slow influence on blood flow. *Nat. Neurosci.* 24, 633–645 (2021).
- Bruzzone, R., Hormuzdi, S. G., Barbe, M. T., Herb, A. & Monyer, H. Pannexins, a family of gap junction proteins expressed in brain. Proc. Natl. Acad. Sci. USA 100, 13644–13649 (2003).
- Pelegrin, P. & Surprenant, A. Pannexin-1 mediates large pore formation and interleukin-1beta release by the ATP-gated P2X7 receptor. *EMBO J.* 25, 5071–5082 (2006).
- 19. Shestopalov, V. I. & Panchin, Y. Pannexins and gap junction protein diversity. *Cell. Mol. Life Sci.* **65**, 376–394 (2008).
- 20. MacVicar, B. A. & Thompson, R. J. Non-junction functions of pannexin-1 channels. *Trends Neurosci.* **33**, 93–102 (2010).
- Gaete, P. S., Lillo, M. A. & Figueroa, X. F. Functional role of connexins and pannexins in the interaction between vascular and nervous system. J. Cell. Physiol. 229, 1336–1345 (2014).
- 22. Bisht, K. et al. Capillary-associated microglia regulate vascular structure and function through PANX1-P2RY12 coupling in mice. *Nat. Commun.* **12**, 5289 (2021).
- Kawamura, H. et al. ATP: a vasoactive signal in the pericytecontaining microvasculature of the rat retina. *J. Physiol.* 551, 787–799 (2003).
- Dahl, G. ATP release through pannexon channels. *Philos. Trans. R.* Soc. Lond. B Biol. Sci. 370, 20140191 (2015).
- 25. Qu, R. et al. Cryo-EM structure of human heptameric pannexin 1 channel. *Cell Res.* **30**, 446–448 (2020).
- Billaud, M. et al. Pannexin1 regulates α1-adrenergic receptormediated vasoconstriction. Circ. Res. 109, 80–85 (2011).
- Crawford, C. et al. Extracellular nucleotides affect pericytemediated regulation of rat in situ vasa recta diameter. Acta Physiol. 202, 241–251 (2011).
- 28. Lacar, B. et al. Neural progenitor cells regulate capillary blood flow in the postnatal subventricular zone. *J. Neurosci.* **32**, 16435–16448 (2012).
- 29. Vanlandewijck, M. et al. A molecular atlas of cell types and zonation in the brain vasculature. *Nature* **554**, 475–480 (2018).
- Mai-Morente, S. P., Marset, V. M., Blanco, F., Isasi, E. E. & Abudara,
 V. A nuclear fluorescent dye identifies pericytes at the neurovascular unit. *J. Neurochem* 157, 1377–1391 (2021).

- Shaw, K. et al. Neurovascular coupling and oxygenation are decreased in hippocampus compared to neocortex because of microvascular differences. *Nat. Commun.* 12. 3190 (2021).
- Hartmann, D. A., Coelho-Santos, V. & Shih, A. Y. Pericyte control of blood flow across microvascular zones in the central nervous system. *Annu. Rev. Physiol.* 84, 331–354 (2022).
- 33. Mishra, A. et al. Imaging pericytes and capillary diameter in brain slices and isolated retinae. *Nat. Protoc.* **9**, 323–336 (2014).
- Ma, W., Hui, H., Pelegrin, P. & Surprenant, A. Pharmacological characterization of pannexin-1 currents expressed in mammalian cells. J. Pharmacol. Exp. Ther. 328, 409–418 (2009).
- Silverman, W., Locovei, S. & Dahl, G. Probenecid, a gout remedy, inhibits pannexin 1 channels. Am. J. Physiol. Cell Physiol. 295, C761–C767 (2008).
- Evans, W. H. & Leybaert, L. Mimetic peptides as blockers of connexin channel-facilitated intercellular communication. *Cell Commun. Adhes.* 14, 265–273 (2007).
- Abudara, V. et al. The connexin43 mimetic peptide Gap19 inhibits hemichannels without altering gap junctional communication in astrocytes. Front. Cell. Neurosci. 8, 306 (2014).
- García-Rodríguez, C. et al. Probenecid, an old drug with potential new uses for central nervous system disorders and neuroinflammation. *Biomedicines* 11, 1516 (2023).
- Isasi, E., Korte, N., Abudara, V., Attwell, D. & Olivera-Bravo, S. Glutaric acid affects pericyte contractility and migration: possible implications for GA-I pathogenesis. *Mol. Neurobiol.* 56, 7694–7707 (2019).
- Boassa, D. et al. Pannexin1 channels contain a glycosylation site that targets the hexamer to the plasma membrane. *J. Biol. Chem.* 282, 31733–31743 (2007).
- Penuela, S. et al. Pannexin 1 and pannexin 3 are glycoproteins that exhibit many distinct characteristics from the connexin family of gap junction proteins. J. Cell Sci. 120, 3772–3783 (2007).
- Cai, C. et al. Stimulation-induced increases in cerebral blood flow and local capillary vasoconstriction depend on conducted vascular responses. *Proc. Natl. Acad. Sci. USA* 115, E5796–E5804 (2018).
- Hørlyck, S., Cai, C., Helms, H. C. C., Lauritzen, M. & Brodin, B. ATP induces contraction of cultured brain capillary pericytes via activation of P2Y-type purinergic receptors. Am. J. Physiol. Heart Circ. Physiol. 320, H699–H712 (2021).
- Lohman, A. W. & Isakson, B. E. Differentiating connexin hemichannels and pannexin channels in cellular ATP release. *FEBS Lett.* 588, 1379–1388 (2014).
- Garré, J. M. et al. FGF-1 induces ATP release from spinal astrocytes in culture and opens pannexin and connexin hemichannels. Proc. Natl. Acad. Sci. USA 107, 22659–22664 (2010).
- Ziganshin, A. U. et al. PPADS selectively antagonizes P2Xpurinoceptor-mediated responses in the rabbit urinary bladder. Br. J. Pharmacol. 110, 1491–1495 (1993).
- Kennedy, C. P1- and P2-purinoceptor subtypes-an update. Arch. Int. Pharmacodyn. Ther. 303, 30-50 (1990).
- 48. Jiang, L. H., Mackenzie, A. B., North, R. A. & Surprenant, A. Brilliant blue G selectively blocks ATP-gated rat P2X(7) receptors. *Mol. Pharm.* **58**, 82–88 (2000).
- 49. Donnelly-Roberts, D. L. et al. [3H] A-804598 is a novel, potent, and selective antagonist radioligand for P2X7 receptors. *Neuro-pharmacology* **56**, 223–229 (2009).
- Timóteo, M. A. et al. ATP released via pannexin-1 hemichannels mediates bladder overactivity triggered by urothelial P2Y6 receptors. *Biochem. Pharmacol.* 87, 371–379 (2014).
- Mamedova, L. K., Joshi, B. V., Gao, Z. G., von Kügelgen, I. & Jacobson, K. A. Diisothiocyanate derivatives as potent, insurmountable antagonists of P2Y6 nucleotide receptors. *Biochem. Pharmacol.* 67, 1763–1770 (2004).

- 52. North, R. A. Molecular physiology of P2X receptors. *Physiol. Rev.* 82. 1013–1067 (2002).
- Kim, S. G. et al. Tumor necrosis factor alpha-induced apoptosis in astrocytes is prevented by the activation of P2Y6, but not P2Y4 nucleotide receptors. *Biochem. Pharmacol.* 65, 923–931 (2003).
- Nortley, R. et al. Amyloid β oligomers constrict human capillaries in Alzheimer's disease via signaling to pericytes. Science 365, eaav9518 (2019).
- 55. Davis, H. & Attwell, D. A tight squeeze: how do we make sense of small changes in microvascular diameter. *J. Physiol.* **601**, 2263–2272 (2023).
- Rancillac, A. et al. Glutamatergic control of microvascular tone by distinct GABA neurons in the cerebellum. *J. Neurosci.* 26, 6997–7006 (2006).
- 57. Lourenço, C. F. et al. Neurovascular coupling in hippocampus is mediated via diffusion by neuronal-derived nitric oxide. *Free Radic. Biol. Med.* **73**, 421–429 (2014).
- Norup Nielsen, A. & Lauritzen, M. Coupling and uncoupling of activity-dependent increases of neuronal activity and blood flow in rat somatosensory cortex. J. Physiol. 533, 773–785 (2001).
- 59. Gsell, W. et al. Differential effects of NMDA and AMPA glutamate receptors on functional magnetic resonance imaging signals and evoked neuronal activity during forepaw stimulation of the rat. *J. Neurosci.* **26**, 8409–8416 (2006).
- 60. Busija, D. W., Bari, F., Domoki, F. & Louis, T. Mechanisms involved in the cerebrovascular dilator effects of N-methyl-d-aspartate in cerebral cortex. *Brain Res Rev.* **56**, 89–100 (2007).
- Chaigneau, E. et al. The relationship between blood flow and neuronal activity in the rodent olfactory bulb. *J. Neurosci.* 27, 6452–6460 (2007).
- 62. Hoffmeyer, H. W., Enager, P., Thomsen, K. J. & Lauritzen, M. J. Nonlinear neurovascular coupling in rat sensory cortex by activation of transcallosal fibers. *J. Cereb. Blood Flow. Metab.* **27**, 575–587 (2007).
- Lecrux, C., Kocharyan, A., Sandoe, C. H., Tong, X. K. & Hamel, E. Pyramidal cells and cytochrome P450 epoxygenase products in the neurovascular coupling response to basal forebrain cholinergic input. J. Cereb. Blood Flow. Metab. 32, 896–906 (2012).
- Domoki, F., Kis, B., Gáspár, T., Bari, F. & Busija, D. W. Cerebromicrovascular endothelial cells are resistant to L-glutamate. Am.
 J. Physiol. Regul. Integr. Comp. Physiol. 295, R1099–R1108 (2008).
- Dossi, E. & Rouach, N. Pannexin 1 channels and ATP release in epilepsy: two sides of the same coin. *Purinergic Signal.* 17, 533–548 (2021).
- Chao, O. Y., Nikolaus, S., Yang, Y. M. & Huston, J. P. Neuronal circuitry for recognition memory of object and place in rodent models. *Neurosci. Biobehav. Rev.* 141, 104855 (2022).
- 67. Denninger, J. K., Smith, B. M. & Kirby, E. D. Novel object recognition and object location behavioral testing in mice on a budget. *J. Vis. Exp.* https://doi.org/10.3791/58593 (2018).
- 68. Shen, J. et al. Neurovascular coupling in the dentate gyrus regulates adult hippocampal neurogenesis. *Neuron* **103**, 878–890.e3 (2019).
- Isakson, B. E. & Thompson, R. J. Pannexin-1 as a potentiator of ligand-gated receptor signaling. Channels 8, 118–123 (2014).
- Qiu, F. & Dahl, G. A permeant regulating its permeation pore: inhibition of pannexin 1 channels by ATP. Am. J. Physiol. Cell Physiol. 296, C250–C255 (2009).
- Iwabuchi, S. & Kawahara, K. Functional significance of the negative-feedback regulation of ATP release via pannexin-1 hemichannels under ischemic stress in astrocytes. *Neurochem. Int.* 58, 376–384 (2011).
- Boyce, A. K., Kim, M. S., Wicki-Stordeur, L. E. & Swayne, L. A. ATP stimulates pannexin 1 internalization to endosomal compartments. *Biochem. J.* 470, 319–330 (2015).

- Boyce, A. K. J. & Swayne, L. A. P2X7 receptor cross-talk regulates ATP-induced pannexin 1 internalization. *Biochem. J.* 474, 2133–2144 (2017).
- DeLalio, L. J. et al. Interaction between pannexin 1 and caveolin-1 in smooth muscle can regulate blood pressure. *Arterioscler*. *Thromb. Vasc. Biol.* 38, 2065–2078 (2018).
- Bao, B. A., Lai, C. P., Naus, C. C. & Morgan, J. R. Pannexin1 drives multicellular aggregate compaction via a signaling cascade that remodels the actin cytoskeleton. *J. Biol. Chem.* 287, 8407–8416 (2012).
- Billaud, M. et al. A molecular signature in the pannexin1 intracellular loop confers channel activation by the α1 adrenoreceptor in smooth muscle cells. Sci. Signal. 8, ra17 (2015).
- Dunaway, L. S. et al. Amount of pannexin 1 in smooth muscle cells regulates sympathetic nerve-induced vasoconstriction. *Hypertension* 80, 416–425 (2023).
- Flores-Muñoz, C. et al. The long-term pannexin 1 ablation produces structural and functional modifications in hippocampal neurons. Cells 11, 3646 (2022).
- 79. Attwell, D. et al. Glial and neuronal control of brain blood flow. *Nature* **468**, 232–243 (2010).
- 80. Lohman, A. W. et al. S-nitrosylation inhibits pannexin 1 channel function. *J. Biol. Chem.* **287**, 39602–39612 (2012).
- 81. Samuels, S. E., Lipitz, J. B., Wang, J., Dahl, G. & Muller, K. J. Arachidonic acid closes innexin/pannexin channels and thereby inhibits microglia cell movement to a nerve injury. *Dev. Neurobiol.* 73, 621–631 (2013).
- Ardiles, A. O. et al. Pannexin 1 regulates bidirectional hippocampal synaptic plasticity in adult mice. Front. Cell. Neurosci. 8, 326 (2014).
- 83. Weilinger, N. L., Tang, P. L. & Thompson, R. J. Anoxia-induced NMDA receptor activation opens pannexin channels via Src family kinases. *J. Neurosci.* **32**, 12579–12588 (2012).
- 84. Thompson, R. J. et al. Activation of pannexin-1 hemichannels augments aberrant bursting in the hippocampus. *Science* **322**, 1555–1559 (2008).
- 85. Retamal, M. A. Connexin and Pannexin hemichannels are regulated by redox potential. *Front. Physiol.* **5**, 80 (2014).
- Orellana, J. A. et al. Modulation of brain hemichannels and gap junction channels by pro-inflammatory agents and their possible role in neurodegeneration. *Antioxid. Redox Signal.* 11, 369–399 (2009).
- Liu, X. et al. General anesthetics have differential inhibitory effects on gap junction channels and hemichannels in astrocytes and neurons. Glia 64, 524–536 (2016).
- 88. Dong, R. et al. Connexin 43 gap junction-mediated astrocytic network reconstruction attenuates isoflurane-induced cognitive dysfunction in mice. *J. Neuroinflamm.* **19**, 64 (2022).
- Park, J. B. & Kim, S. J. Anti-hypertensive effects of probenecid via inhibition of the α-adrenergic receptor. *Pharm. Rep.* 63, 1145–1150 (2011).
- Xiong, X. X. et al. Probenecid protects against transient focal cerebral ischemic injury by inhibiting HMGB1 release and attenuating AQP4 expression in mice. *Neurochem. Res.* 39, 216–224 (2014).
- Freitas-Andrade, M. et al. Pannexin1 knockout and blockade reduces ischemic stroke injury in female, but not in male mice. Oncotarget 8, 36973–36983 (2017).
- Wei, R. et al. Probenecid protects against cerebral ischemia/ reperfusion injury by inhibiting lysosomal and inflammatory damage in rats. Neuroscience 301, 168–177 (2015).
- Bell, R. D. et al. Pericytes control key neurovascular functions and neuronal phenotype in the adult brain and during brain aging. Neuron 68, 409–427 (2010).

- Pandey, K. et al. Neuronal activity drives IGF2 expression from pericytes to form long-term memory. *Neuron* 111, 3819–3836.e8 (2023).
- 95. Prochnow, N. et al. Pannexin1 stabilizes synaptic plasticity and is needed for learning. *PLoS ONE* **7**, e51767 (2012).
- Gajardo, I. et al. Lack of pannexin 1 alters synaptic GluN2 subunit composition and spatial reversal learning in mice. Front. Mol. Neurosci. 11, 114 (2018).
- 97. Obot, P. et al. Astrocyte and neuronal Panx1 support long-term reference memory in mice. ASN Neuro 15, 17590914231184712 (2023).
- 98. Uemura, M. T., Maki, T., Ihara, M., Lee, V. M. Y. & Trojanowski, J. Q. Brain microvascular pericytes in vascular cognitive impairment and dementia. *Front. Aging Neurosci.* **12**, 80 (2020).
- Korte, N. et al. Inhibiting Ca2+ channels in Alzheimer's disease model mice relaxes pericytes, improves cerebral blood flow and reduces immune cell stalling and hypoxia. *Nat. Neurosci.* https:// doi.org/10.1038/s41593-024-01753-w (2024).
- Qu, Y. et al. Pannexin-1 is required for ATP release during apoptosis but not for inflammasome activation. *J. Immunol.* 186, 6553–6561 (2011).
- Dvoriantchikova, G. et al. Genetic ablation of Pannexin1 protects retinal neurons from ischemic injury. PLoS ONE 7, e31991 (2012).
- Cuervo, H. et al. PDGFRβ-P2A-CreERT2 mice: a genetic tool to target pericytes in angiogenesis. Angiogenesis 20, 655–662 (2017).
- 103. Mai-Morente, S. P. et al. Pericyte mapping in cerebral slices with the far-red fluorophore TO-PRO-3. *Bio Protoc.* **11**, e4222 (2021).
- Giaume, C., Orellana, J. A., Abudara, V. & Sáez, J. C. Connexinbased channels in astrocytes: how to study their properties. Methods Mol. Biol. 814, 283–303 (2012).
- 105. Peters, B. P. & Goldstein, I. J. The use of fluorescein-conjugated Bandeiraea simplicifolia B4-isolectin as a histochemical reagent for the detection of alpha-D-galactopyranosyl groups. Their occurrence in basement membranes. Exp. Cell Res. 120, 321–334 (1979).
- Laitinen, L. Griffonia simplicifolia lectins bind specifically to endothelial cells and some epithelial cells in mouse tissues. *Histochem J.* 19, 225–234 (1987).
- Harrison, C. H. et al. A novel method to visualise the threedimensional organisation of the human cerebral cortical vasculature. J. Anat. 232, 1025–1030 (2018).
- Yardeni, T., Eckhaus, M., Morris, H. D., Huizing, M. & Hoogstraten-Miller, S. Retro-orbital injections in mice. *Lab. Anim.* 40, 155–160 (2011).
- Tian, P. et al. Cortical depth-specific microvascular dilation underlies laminar differences in blood oxygenation leveldependent functional MRI signal. Proc. Natl. Acad. Sci. USA 107, 15246–15251 (2010).
- Takano, T. et al. Rapid manifestation of reactive astrogliosis in acute hippocampal brain slices. Glia 62, 78–95 (2014).
- Sargent, S. M. et al. Endothelial structure contributes to heterogeneity in brain capillary diameter. Vasc. Biol. 5, e230010 (2023).
- Leger, M. et al. Object recognition test in mice. Nat. Protoc. 8, 2531–2537 (2013).
- 113. Lueptow, L. M. Novel object recognition test for the investigation of learning and memory in mice. *J. Vis. Exp.* **126**, 55718 (2017).

Acknowledgements

This work was supported by the Comisión Sectorial de Investigación Científica—Universidad de la República Oriental del Uruguay [CSIC—UdelaR, Uruguay, grant numbers: 22320200200022UD (S.M.), ID139 (E.I.), 22520220100095UD (N.V.), ID48 and 22520220100243UD (V.A.) and doctoral fellowship (S.M.)], by the Agencia Nacional de

Investigación e Innovación-Ministerio de Educación y Cultura [ANII-MEC-Uruguay, grant number FCE 1 2017 1 136103 (V.A.) and doctoral fellowships (S.M. and A.R.)], by Dirección Nacional de Innovación, Ciencia y Tecnología [DICYT-MEC, Uruguay, grant number II/FVF/2019/ 030 (E.I)], by the Instituto de Investigaciones Biológicas Clemente Estable [IIBCE-MEC-Uruguay (S.O.-B.)] and by the Programa de Desarrollo de las Ciencias Básicas (PEDECIBA, Uruguay). The authors thank Engineer A. Canabal (MSc) and Drs. Michael Bennett, PhD*, JC Sáez, A. Cayota and R. Alonso for scientific advice, and the Unidad de Biotecnología de Animales de Laboratorio—Institut Pasteur de Montevideo (UBAL-IP Montevideo), Unidad de Reactivos para Biomodelos de Experimentación (URBE), FUNDACIBA, Unidad de Microscopía Confocal, and Centro de Investigaciones Biomédicas (CEINBIO) from the Facultad de Medicina-Universidad de la República Oriental del Uruguay, and Plataforma de Microscopía Confocal y Epifluorescencia-Instituto de Investigaciones Biológicas Clemente Estable [IIBCE-MEC-Uruguay] for technical assistance. * Deceased on November 16th, 2023.

Author contributions

S.M. and V.A. conceived the project. S.M. designed, performed, and analyzed ex vivo, in vivo, and calcium imaging experiments with contributions from V.A. Culture experiments were designed, performed, and analyzed by E.I. and S.O.-B. whereas A.R. and N.V. designed, performed, and analyzed extracellular ATP measurements. Some of the functional experiments were designed and conducted by G.B. All authors commented on the manuscript, V.A. prepared figures, and S.M. and V.A. wrote the manuscript with inputs from E.I., A.R., G.B., and N.V.

Competing interests

The authors declare no competing interests.

Additional information

Supplementary information The online version contains supplementary material available at https://doi.org/10.1038/s41467-025-61312-0.

Correspondence and requests for materials should be addressed to Verónica Abudara.

Peer review information *Nature Communications* thanks Roger Thompson and the other anonymous reviewer(s) for their contribution to the peer review of this work. A peer review file is available.

Reprints and permissions information is available at http://www.nature.com/reprints

Publisher's note Springer Nature remains neutral with regard to jurisdictional claims in published maps and institutional affiliations.

Open Access This article is licensed under a Creative Commons Attribution-NonCommercial-NoDerivatives 4.0 International License, which permits any non-commercial use, sharing, distribution and reproduction in any medium or format, as long as you give appropriate credit to the original author(s) and the source, provide a link to the Creative Commons licence, and indicate if you modified the licensed material. You do not have permission under this licence to share adapted material derived from this article or parts of it. The images or other third party material in this article are included in the article's Creative Commons licence, unless indicated otherwise in a credit line to the material. If material is not included in the article's Creative Commons licence and your intended use is not permitted by statutory regulation or exceeds the permitted use, you will need to obtain permission directly from the copyright holder. To view a copy of this licence, visit https://creativecommons.org/licenses/by-nc-nd/4.0/.

© The Author(s) 2025